ACSNANO

www.acsnano.org

ARTICLE

Treating Autoimmune Inflammatory Diseases with an siERN1-Nanoprodrug That Mediates Macrophage Polarization and Blocks Toll-like Receptor Signaling

Naibo Feng, Li Liang, Mengtian Fan, Yu Du, Cheng Chen, Rong Jiang, Dongsheng Yu, Yuyou Yang, Mengying Zhang, Lin Deng, Xingyue Li, Nana Geng, Menglin Xian, Qizhong Qin, Xiaoli Li, Qiaoyan Tan, Fengtao Luo, Fangzhou Song, Huabing Qi, Yangli Xie, and Fengjin Guo*

Cite This: https://doi.org/10.1021/acsnano.1c03726

Read Online

ACCESS | Metrics & More | Article Recommendations | Supporting Information

ABSTRACT: The clinical application of small interfering RNA (siRNA) drugs provides promising opportunities to develop treatment strategies for autoimmune inflammatory diseases. In this study, siRNAs targeting the endoplasmic reticulum to nucleus signaling 1 (*ERN1*) gene (siERN1) were screened. Two cationic polymers, polyethylenimine (PEI) and poly(β-amino amine) (PBAA), which can improve the efficiency of the siRNA transfection, were used as siERN1 delivery carriers. They were implemented to construct a nanodrug delivery system with macrophage-targeting ability and dual responsiveness for the treatment of autoimmune inflammatory diseases. In terms of the mechanism, siERN1 can regulate the intracellular calcium ion concentration by interfering with the function of inositol 1,4,5-trisphosphate receptor 1/3 (IP3R1/3) and thus inducing M2 polarization of macrophages. Furthermore, siERN1-nanoprodrug [FA (folic acid)−PEG−R(RKKRRQRRR)−NPs(ss−PBAA−PEI)@siERN1] acts as a conductor of macrophage polarization by controlling the calcium ion concentration and is an inhibitor of MyD88-dependent Toll-like receptor signaling. The results revealed that the FA−PEG−R−NPs@siERN1 has universal biocompatibility, long-term drug release responsiveness, superior targeting properties, and therapeutic effects in mouse collagen-induced arthritis and inflammatory bowel disease models. In conclusion, this study reveals a potential strategy to treat autoimmune inflammatory disorders.

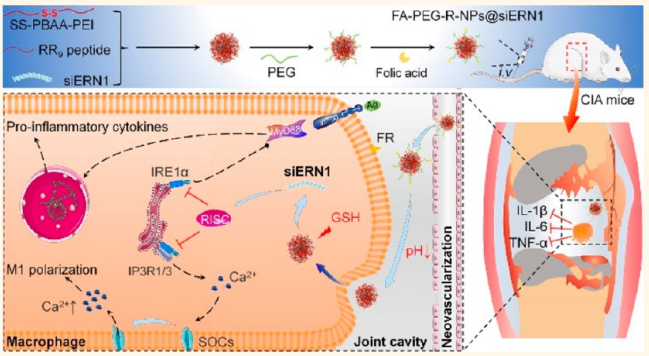

KEYWORDS: *autoimmune inflammatory diseases, siERN1, toll-like receptor signaling, rheumatoid arthritis, inflammatory bowel disease, macrophage polarization, nanoprodrug*

Autoimmune diseases are caused by the body's immune response to self-antigens, which results in damage to the body's tissues.[1,2] Among them, rheumatoid arthritis (RA) and inflammatory bowel disease (IBD) are mainly characterized by inflammation. However, the pathogenesis of these diseases remains unclear. In general, the imbalance of immune homeostasis and cytokines is an important mechanism for the occurrence and development of disease.[3,4] The latest treatment guidelines that are issued by the European League Against Rheumatism recommend using disease-modifying antirheumatic drugs as the first line of treatment while emphasizing the important role of glucocorticoids and biological agents during clinical treatment.[5,6] Although these drugs have good therapeutic effects in clinical applications, the guidelines still point out that there are certain limitations to their clinical applications, including gastrointestinal reactions, bone marrow transplantation, drug resistance, and the occurrence of malignant tumors.[7−9] Therefore, the development of drugs that can reduce side effects is imminent.

Received: May 3, 2021
Accepted: September 27, 2021

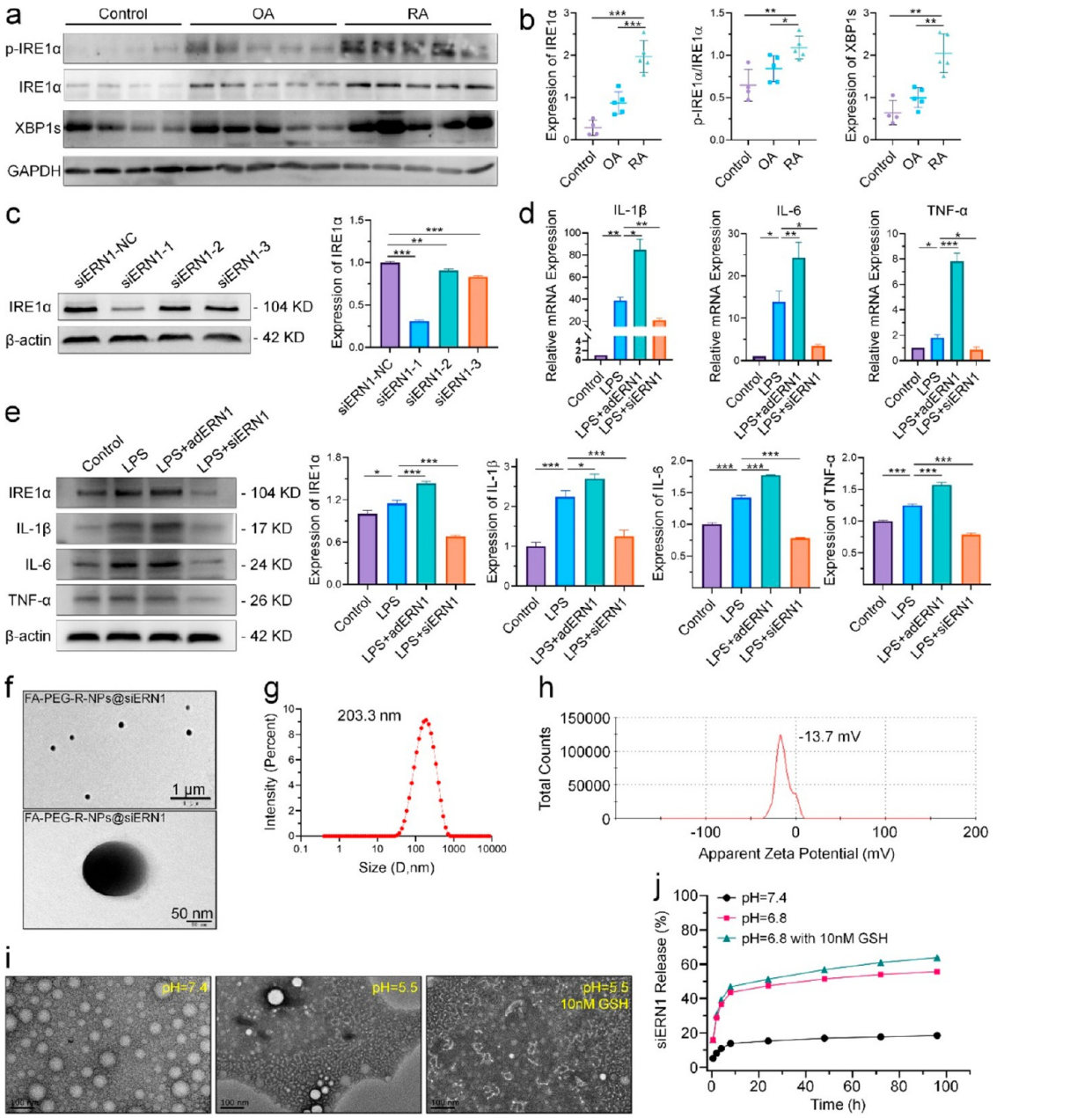

Figure 1. Role of IRE1α in RA, screening and characterization of siERN1, and construction and characterization of FA−PEG−R−NPs@siERN1. (a) The expression of IRE1α in joint synovial tissue of control ($N = 4$), OA patients ($N = 5$), or RA patients ($N = 5$) was detected by Western blot and (b) semiquantitative analysis results. (c) Screening and identification of the siERN1 knockdown efficiency. The role of siERN1 in an LPS-induced M1 polarization model of RAW 264.7 cells was detected by (d) RT-qPCR and (e) Western blot. (f) The morphology and particle size of FA−PEG−R−NPs@siERN1 were observed by TEM. (g) The hydrodynamic size of FA−PEG−R−NPs@siERN1 was detected by DLS. (h) Apparent zeta potential of FA−PEG−R−NPs@siERN1. (i) Morphological changes of FA−PEG−R−NPs@siERN1 under different conditions (pH and GSH) were observed by TEM. (j) siERN1 release behavior of FA−PEG−R−NPs@siERN1 under different pH conditions in the presence or absence of GSH. N.S., not significant; *$P < 0.05$, **$P < 0.01$, and ***$P < 0.001$.

Recently, the unfolded protein response (UPR) has received significant attention because of its important role in inflammatory diseases.[10−12] Inositol-requiring enzyme 1α (IRE1α), which is encoded by the endoplasmic reticulum to nucleus signaling 1 (*ERN1*) gene, is an important molecular sensor for UPR and has a wide range of canonical and noncanonical functions in eukaryotic cells. IRE1α initiates the most conserved UPR signaling pathway and is involved in the regulation of calcium transport in the endoplasmic reticulum (ER), as well as mitochondrial bioenergetics and physiology. Studies have shown that IRE1α controls ER hemostasis and cell survival through a variety of mechanisms. The activation of IRE1α promotes the production of a variety of inflammatory cytokines, such as tumor necrosis factor (TNF)-α, IL-6, and IL-1β. In addition, TRAF6-mediated IRE1α ubiquitination regulates Toll-like receptor (TLR)-induced IRE1α activation in pro-inflammatory cytokine production.[13,14] The specific IRE1α inhibitor 4U8C can improve the symptoms of inflammatory arthritis in mouse models.[15] Therefore, the design of a highly effective small interfering RNA (siRNA) targeting *ERN1* (siERN1) that specifically knocks down the expression of

https://doi.org/10.1021/acsnano.1c03726
ACS Nano XXXX, XXX, XXX−XXX

IRE1α and its effect may be used as a potential strategy to treat RA or other autoimmune inflammatory diseases.

The effectiveness and efficiency of polyethylenimine (PEI) and poly(β-amino amine) (PBAA) as nonviral gene drug carriers have been verified in many previous studies.[16−19] In this study, we devised a specific nanomaterial that can achieve targeted siRNA drug delivery. In essence, the siERN1 with the best inhibition efficiency was identified. Thereafter, the disulfide-containing cationic core ss−PBAA−PEI (NPs) was synthesized, and a cell-penetrating peptide RKKRRQRRR (R) was coupled to the core, resulting in the formation of R−NPs. siERN1 was loaded onto the R−NPs to enable the assembly of the drug carrier core (R−NPs@siERN1). Next, the core was modified with PEG (PEG−R−NPs@siERN1). The presence of the PEG shell improves the biocompatibility of the nanomedicine. Additionally, the macrophage-specific targeting ligand folic acid (FA) was grafted through the PEG shell to complete the final nanomedicine assembly (FA−PEG−R−NPs@siERN1). This drug delivery system effectively avoids nuclease cleavage of siRNA and improves the effectiveness of the siRNA drug through targeted delivery to the immune cells. Through this investigation, it was verified that the siERN1-nanoprodrug has a suitable particle size as well as superior biocompatibility and pH/redox responsiveness.

The polarization of macrophages participates in many inflammatory diseases. Polarization is associated with the multiple roles of macrophages in organisms. M1 macrophages express various pro-inflammatory mediators, such as TNF-α, IL-1, and IL-6, whereas M2 macrophages express molecules such as CD206, arginase1 (Arg1), and IL-10. M1 and M2 macrophages can be interconverted in their specific microenvironment.[20−22] In addition, many vital transcription factors are involved in macrophage polarization, including interferon-regulatory factors (IRFs), signal transducers and activators of transcription (STATs), and nuclear factor (NF)-κB. These factors interact with each other and regulate macrophage phenotypes in various inflammatory diseases.[23,24] Identification of specific targeted pathways and molecules in the local microenvironment that transform macrophages into an appropriate phenotype can facilitate regulation of the occurrence and development of inflammatory diseases.

In our efforts to clarify the molecular mechanism of FA−PEG−R−NPs@siERN1 targeting the macrophages for autoimmune inflammatory diseases treatment, siERN1 was found to affect the function of inositol 1,4,5-trisphosphate receptor (InsP3R, IP3R)1/3 by downregulating the expression of *ERN1* and its interaction with IP3R1/3. This in turn interferes with the polarization direction of the macrophages by modulating the intracellular Ca^{2+} concentration in the macrophages. Furthermore, FA−PEG−R−NPs@siERN1 serves as an inhibitor of the myeloid differentiation factor 88 (MyD88)-dependent TLR signaling pathway to relieve inflammation. This study confirmed that the nanomedicine effectively inhibits the severity and progression of the disease, reduces inflammation, and effectively protects the joints and intestines in collagen-induced arthritis (CIA) and dextran sulfate sodium salt (DSS)-induced IBD models, respectively, thus suggesting that the same siRNA-nanoprodrug treatment may be applicable for various inflammatory diseases and also provides a reliable method for drug delivery and gene therapy in clinical applications.

RESULTS AND DISCUSSION

Expression and Phosphorylation Level of IRE1α in RA Patients. To explore the expression profile of IRE1α in RA patients, a quantitative analysis of the clinical samples was conducted through Western blotting (Figure 1a and b, Supplementary Figure 1). The data demonstrate that the level of IRE1α in osteoarthritis (OA) and RA cartilage was upregulated and was markedly increased in the RA cartilage compared to that in the normal cartilage. Additionally, the phosphorylation level of IRE1α was significantly increased in the RA samples, representing a higher activation level in the RA cartilage tissue. Moreover, the expression of XBP 1s, which is produced through cleavage by phosphorylation-activated IRE1α (p-IRE1α) during ER stress, was relatively high in the RA cartilage. Indeed, the canonical and noncanonical functions of IRE1α are involved in the pathogenesis of multiple inflammation-related diseases as reported in the literature.[13,14,25−27] The canonical function of IRE1α can be activated, and it cleaves XBP1u to generate XBP 1s under ER stress while promoting the release of pro-inflammatory factors in macrophages. Thus, the expression and phosphorylation of IRE1α are related to the pathogenesis and development of RA.

Design, Construction, and Characterization of the siERN1-Nanoprodrug Delivery System. siERN1 was designed and synthesized by Sangon Biotech Co., Ltd. (Shanghai, China). The inhibitory efficiency of siERN1-1 was approximately 75% in HEK 293 and RAW 264.7 cells (Figure 1c and e). Therefore, siERN1-1 was selected as the siRNA drug for the subsequent experiments. Overexpression of *ERN1* with the adenovirus (Supplementary Figure 2) increased the expression of the pro-inflammatory cytokines IL-1β, IL-6, and TNF-α induced by lipopolysaccharide (LPS), whereas knockdown of *ERN1* with siRNA reduced the expression of these pro-inflammatory cytokines (Figure 1d and e). Consistent results were obtained in THP-1 cells (Supplementary Figure 3).

The inflammatory microenvironment of the RA- and IBD-affected areas is slightly acidic.[28] In addition, the macrophages in RA patients are overactivated,[29,30] the folate receptors on the cell surface are overexpressed,[31,32] and the content of antioxidants such as glutathione (such as GSH) inside the cells is increased.[33] On this basis, we designed a specific nanomaterial that could achieve targeted siERN1 drug delivery to the macrophages (Supplementary Scheme 1). During the process of assembling the nanomedicine, the intermediate products were characterized by using gel permeation chromatography and hydrogen nuclear magnetic spectroscopy, to provide the basis for the correct assembly of the final product (Supplementary Figures 4 and 5). After the final assembly of the siERN1-nanoprodrug, it was characterized by using various techniques. First, the size and appearance of the nanomedicine were observed by transmission electron microscopy (TEM). The TEM data reveal that the final synthesized nanomedicine, FA−PEG−R−NPs@siERN1, is spherical with a particle size of approximately 110.0 nm (Figure 1f). Using dynamic light scattering (DLS), the hydrodynamic size was found to be 203.3 nm (Figure 1g). In addition, the apparent zeta potential of FA−PEG−R−NPs@siERN1 was determined to be −13.7 mV (Figure 1h). Blood is alkaline, and protein is negatively charged in an alkaline solution; thus, protein exists in the form of anions in blood. Therefore, the negative potential on the surface of FA−PEG−R−NPs@siERN1 prevents the adhesion of the nanomedicine to the nonspecific protein in the blood circulation, and at the same

https://doi.org/10.1021/acsnano.1c03726
ACS Nano XXXX, XXX, XXX−XXX

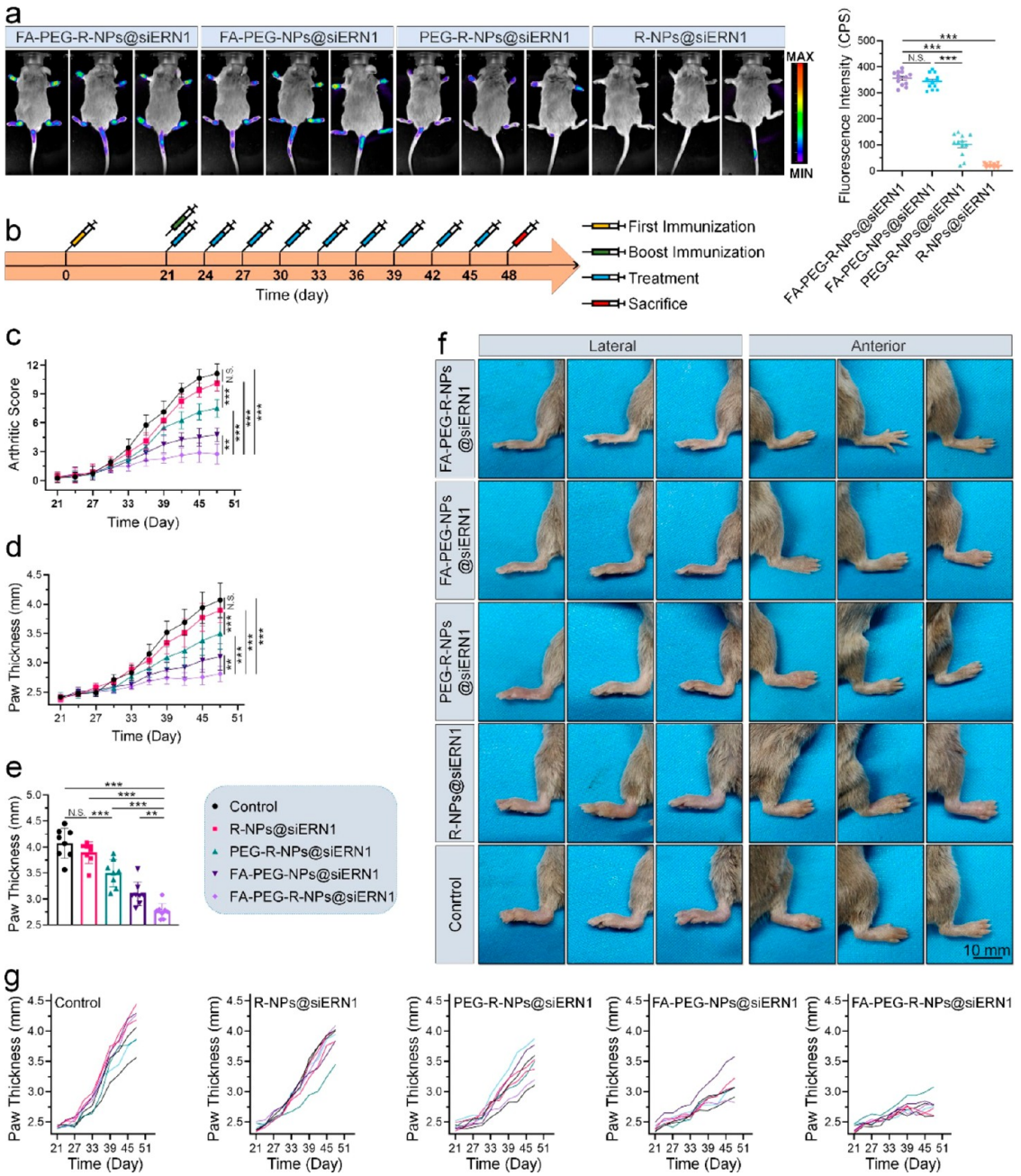

Figure 2. Therapeutic effect of FA−PEG−R−NPs@siERN1 in the CIA model. (a) Different siERN1 preparations labeled with ICG were injected into the tail vein, and the fluorescence aggregation of the nanoprodrugs was observed by the *in vivo* imaging system at 12 h. (b) Schematic diagram of the CIA model building and treatment schedule. (c) Change trend of arthritis score and (d) hind paw thickness of mice in each group every 3 days ($N = 8$). (e) The thickness and (f) appearance of the hind paws of each mouse on the 48th day. (g) Trend of the thickness of the hind paw of each mouse during the treatment. N.S., not significant; *$P < 0.05$, **$P < 0.01$, and ***$P < 0.001$.

time, it provides good dispersion of the nanomedicine in the blood. Subsequently, the morphological changes in the designed nanoprodrug under different conditions were observed by using TEM. As shown in Figure 1i, under neutral pH conditions, the nanomedicine appears as uniformly dispersed spherical particles with a particle size of approximately 100.0 nm. The nanomedicine was partially degraded under the acidic conditions (pH 5.5) and was completely degraded under acidic conditions and the presence of GSH, showing no obvious nanoparticle structure. The data demonstrate that the nanomedicine is sensitive to acidic pH and reducing conditions, and its structure is destroyed under acidic conditions and the presence of GSH.

To further verify this characteristic, the drug release behavior of FA−PEG−R−NPs@siERN1 under different conditions was characterized. As shown in Figure 1j, under neutral conditions, siERN1 is slowly released from FA−PEG−R−NPs@siERN1, and the total amount released is extremely low, reaching approximately 18% in 96 h. However, under acidic conditions (pH 6.8), the rapid release behavior of siERN1 can be observed. The amount of drug released reached 36% at 4 h and 56% at 96 h. As expected, under acidic conditions in the presence of the GSH, FA−PEG−R−NPs@siERN1 demonstrated the fastest drug release behavior, with 40% of the drug being released in 4 h and the final release amount of approximately 64%. In addition,

https://doi.org/10.1021/acsnano.1c03726
ACS Nano XXXX, XXX, XXX−XXX

the MTT and hemolysis experiments confirmed that the siERN1-nanoprodrug has good biocompatibility (Supplementary Figures 6 and 7). Thus, the nanoprodrug has a suitable particle size and apparent zeta potential, superior biocompatibility, and good responsiveness. These characteristics laid the foundation for the subsequent experimental studies.

Therapeutic Effect of FA−PEG−R−NPs@siERN1 in the CIA Model. The targeting of FA−PEG−R−NPs@siERN1 was verified through an *in vivo* imaging system before it was used to treat CIA mice. The siERN1 preparations were labeled with ICG (Supplementary Figure 8). Strong fluorescence signals were observed in the limbs of the mice in the ICG−FA−PEG−R−NPs@siERN1 group and ICG−FA−PEG−NPs@siERN1 group (Figure 2a). The intensity of the fluorescence signal corresponds to the amount of siERN1-nanoprodrug that accumulated in the joint. Therefore, owing to the presence of FA, FA−PEG−R−NPs@siERN1 and FA−PEG−NPs@siERN1 can accurately target the siERN1 drugs to the joints that are inflamed. Although a small amount of fluorescence aggregation signal was found in the limbs of the mice in the ICG−PEG−R−NPs@siERN1 group, there was still a large difference in the fluorescence intensity compared to the ICG−FA−PEG−R−NPs@siERN1 group and the ICG−FA−PEG−NPs@siERN1 group. However, no obvious fluorescence signal was observed in the R−NPs@siERN1 group. Thus, we speculated that the presence of PEG prolongs the circulation time of the siERN1 prodrugs in the blood. Therefore, without the protection of the PEG shell, R−NPs@siERN1 may be quickly metabolized out of the body. In summary, the presence of a PEG shell is necessary for the siERN1-nanoprodrug. On one hand, it can prolong the circulation time of the siERN1-nanoprodrug in the body. On the other hand, FA can also be grafted with PEG to achieve targeted delivery of the siERN1-nanoprodrugs.

In addition, the biodistribution of siERN1 nanoprodrugs in various organs has been verified again. siERN1 was first labeled with Cy5 and then encapsulated within the nanocarriers, i.e., four Cy5-siERN1-nanoprodrugs (FA−PEG−R−NPs@Cy5-siERN1, FA−PEG−NPs@Cy5-siERN1, PEG−R−NPs@Cy5-siERN1, and R−NPs@Cy5-siERN1) were assembled (Supplementary Figure 9). As shown in Supplementary Figure 10a and b, the siERN1-nanoprodrugs mainly aggregate in the liver and kidney. Consistent with the previous *in vivo* imaging data, strong fluorescence signals were observed in the limbs and/or joints of mice in the FA−PEG−R−NPs@Cy5-siERN1 and FA−PEG−NPs@Cy5-siERN1 groups, followed by those in the mice from the PEG−R−NPs@Cy5-siERN1 group; almost no fluorescence signals were observed in case of the mice from the R−NPs@Cy5-siERN1 group.

In view of the observation that there is no difference between the FA−PEG−R-NPs@Cy5-siERN1 and PEG−R−NPs@Cy5-siERN1 groups in the affected joint area, the ability of each siERN1 preparation to enter the cells was further tested *via* a cell uptake experiment. As shown in Supplementary Figure 11a, the samples from the R−NPs@siERN1 group showed the strongest fluorescence intensity at 1 h, while those in the FA−PEG−NPs@siERN1 group showed the weakest fluorescence intensity. At 2 h, the fluorescence intensity of the samples from the FA−PEG−R−NPs@siERN1 and PEG−R−NPs@siERN1 groups increased significantly compared with the fluorescence intensity at the 1 h time point, but the fluorescence intensity of the samples from the FA−PEG−NPs@siERN1 group did not increase significantly (Supplementary Figure 11b and c). It is suggested that penetrating peptides can notably enhance the ability of siERN1-nanoprodrugs to enter macrophages.

Pharmacokinetics is an important evaluation indicator for drug development. The Cy5-labeled siERN1-nanoprodrugs were injected into the tail vein of mice, and the plasma fluorescence intensity at different time points was measured to evaluate the siERN1 contents in the plasma. As shown in Supplementary Figure 12, stronger fluorescence intensity was observed at the first three time points (15 min, 30 min, and 1 h), representing a higher siERN1 content in plasma. The plasma siERN1 concentration decreased over time. Among them, the R−NPs@siERN1 group showed the most significant reduction in the plasma siERN1 concentration at the 6 h time point. This may be due to the absence of PEG-protected drugs; because the drugs from these groups lacked PEG, they were quickly eliminated from the body. The presence of PEG prolongs the circulation time of the drug in the body and leads to a longer-lasting fluorescent signal. The samples in the FA−PEG−R−NPs@siERN1 and FA−PEG−NPs@siERN1 groups showed no significant difference in the trend of change in the plasma siERN1 concentration; a certain concentration of siERN1 was still maintained in the plasma at the 24 h time point. However, the PEG−NPs@siERN1 group showed a slower change in the trend of siERN1 concentration. It is speculated that due to the targeting effects of FA, in the FA−PEG−R−NPs@siERN1 and FA−PEG−NPs@siERN1 groups, the drugs may be retained more quickly in the affected joint area.

Subsequently, the drug efficacy was verified in the CIA model according to the design plan shown in Figure 2b. Figure 2c illustrates that the disease progression control by the siERN1 preparations in each group was comprehensively evaluated by using the arthritis score. The control group showed natural disease progression in the CIA mice and received a final score of 11.1, which represents the most severe arthritis performance. Correspondingly, the arthritis score of the mice in the FA−PEG−R−NPs@siERN1 treatment group showed a slow upward trend, and the average score was only 2.7 in the last treatment, indicating the best treatment effect. Although not as good as the FA−PEG−R−NPs@siERN1 group, relatively good treatment effects were observed in the FA−PEG−NPs@siERN1 group. It was revealed that the average last arthritis score was approximately 4.8. The difference in the efficacy between the two groups may be attributed to the existence of the cell-penetrating peptides. These peptides can assist the nanocore to pass through the cell membrane, allowing more siERN1 to enter the cell and improving its transfection efficiency. Compared with the FA−PEG−R−NPs@siERN1 group, the PEG−R−NPs@siERN1 treatment group showed poor targeting owing to the lack of FA, leading to a significant decrease in the therapeutic effect. Interestingly, there was no significant difference in the arthritic scores between the R−NPs@siERN1 group and the control group. Although nanomaterials are used as carriers to package siERN1, the nanocore lacks the protection of the PEG shell; thus, it is unable to stably exist in the blood circulation and is immediately excreted from the body. In contrast, the naked penetrating peptide may bring the nanocore into nontarget cells, causing the off-target phenomenon of siERN1 and directly affecting the therapeutic effect.

In addition, the thickness of the hind paws of the mice during the entire treatment period was measured. Overall, the change trend of the hind paw thickness in each group roughly corresponds to the change trend of the arthritis score (Figure 2d). Images of both hind paws from the mice were collected on

https://doi.org/10.1021/acsnano.1c03726
ACS Nano XXXX, XXX, XXX−XXX

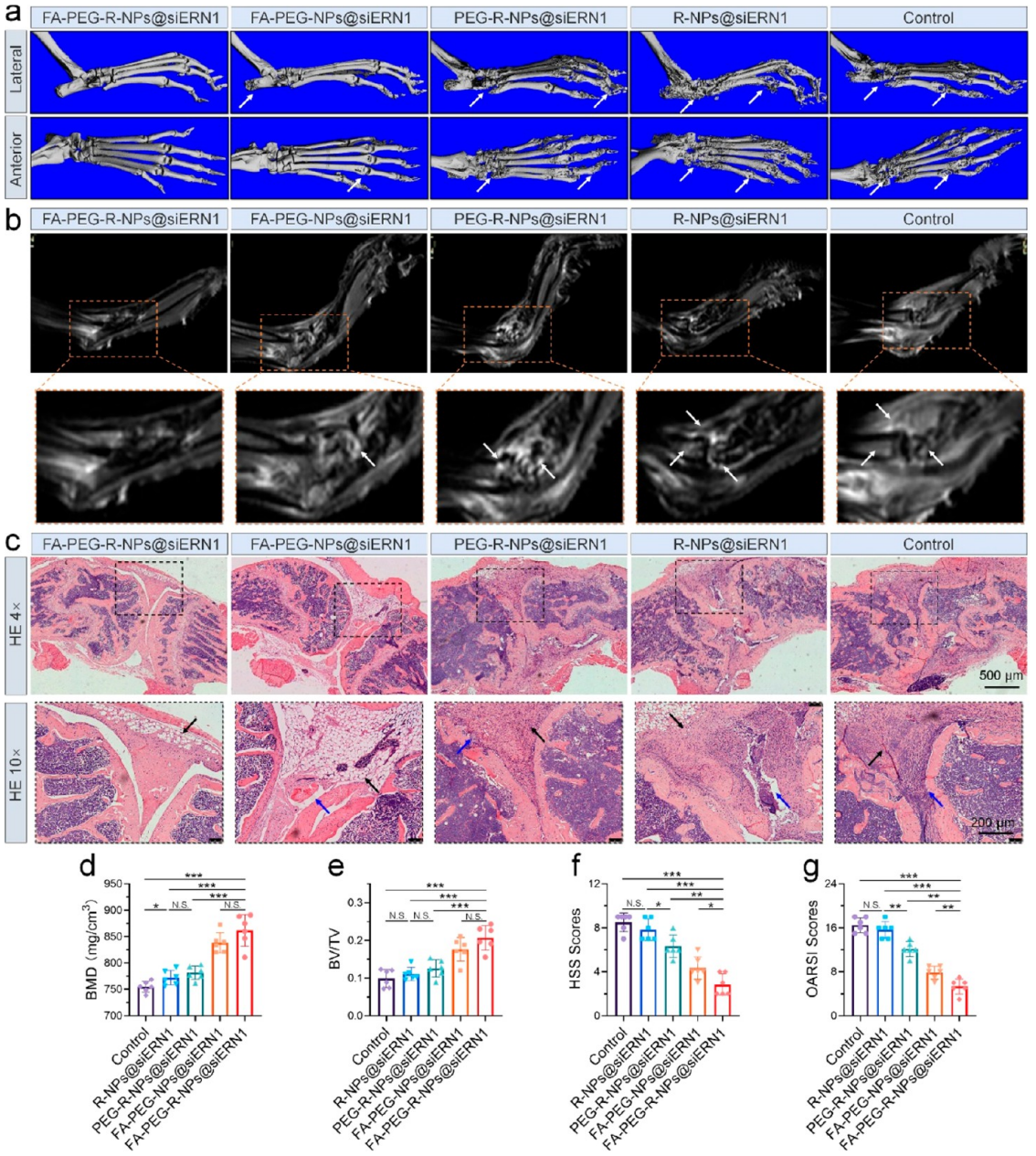

Figure 3. Protective effect of FA−PEG−R−NPs@siERN1 on cartilage and subchondral bone in CIA mice. (a) The hind paws were scanned and three-dimensionally reconstructed by micro-CT to observe the joint shape and bone mass. (b) Evaluation of edema tissue and bone marrow edema of the hind paw by MRI. (c) The morphology of articular cartilage and synovial invasion were observed by HE staining of mice knee joints. (d) BMD and (e) BV/TV data obtained by micro-CT were used to quantitatively analyze the bone mass of the hind paw. Quantification of HE staining by (f) HSS scores and (g) OARSI scores and evaluation of the effect of FA−PEG−R−NPs@siERN1 on articular cartilage protection and synovial inflammation inhibition. N.S., not significant; *$P < 0.05$, **$P < 0.01$, and ***$P < 0.001$.

day 48, and the difference in the hind paw thickness was analyzed (Figure 2e and f). The results showed that FA−PEG−R−NPs@siERN1 significantly inhibited the swelling of the hind paws and the joints of the mice, with an average hind paw thickness of 2.81 mm. However, the average thicknesses of the hind paws of the mice in the FA−PEG−NPs@siERN1 group, PEG−R−NPs@siERN1 group, R−NPs@siERN1 group, and control group were 3.10, 3.49, 3.89, and 4.07 mm, respectively. To more intuitively reflect the treatment effect in each treatment group, a curve of the hind paw thickness of each mouse during the treatment was constructed (Figure 2g). In summary, FA−PEG−R−NPs@siERN1 significantly slows down RA progression and effectively inhibits the swelling of the hind paws and joints of CIA mice, thus demonstrating a superior therapeutic effect.

Protective Effects of FA−PEG−R−NPs@siERN1 on the Articular Cartilage in the CIA Model. To verify the protective effect of FA−PEG−R−NPs@siERN1 on the joints, the hind limbs of the mice were scanned and reconstructed by performing micro-computed tomography (micro-CT). As shown in Figure 3a, the joint surface of the mice in the FA−PEG−R−NPs@siERN1 group is smooth and flat, and there is no sign of bone loss. In contrast, different degrees of joint destruction were observed in the other groups, which were manifested as blurred joints or even joint fusion. Quantitative analysis of the bone mineral density (BMD) (Figure 3d) and

https://doi.org/10.1021/acsnano.1c03726
ACS Nano XXXX, XXX, XXX−XXX

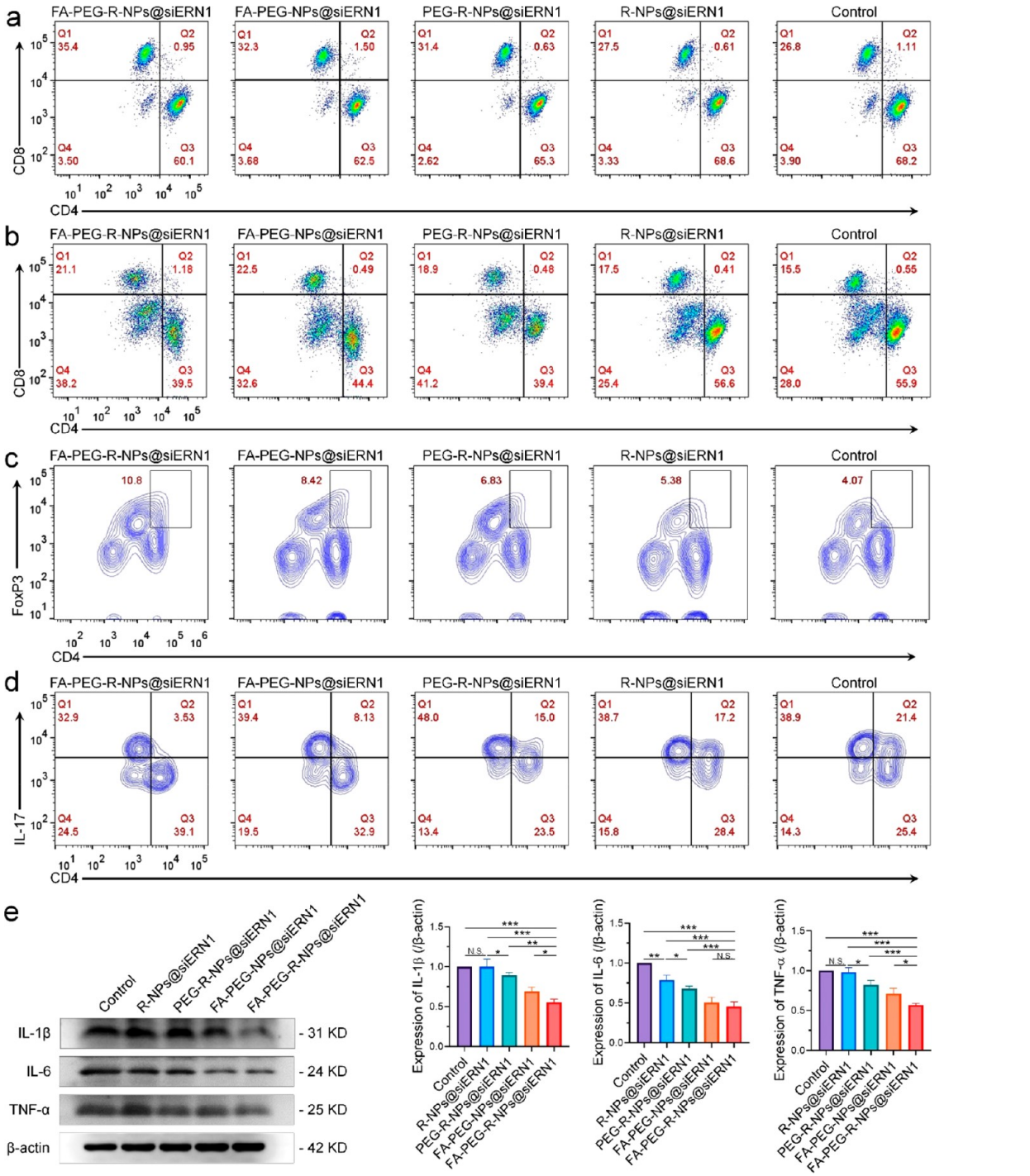

Figure 4. Immunomodulatory and inflammation inhibitory effects of FA−PEG−R−NPs@siERN1 on CIA mice. The proportions of $CD45^+CD3^+CD4^+$ T cells and $CD45^+CD3^+CD8^+$ T cells in (a) lymph nodes T cells and (b) splenic T cells were detected by flow cytometry. The proportions of (c) $CD45^+CD3^+CD4^+FoxP3^+$ T cells and (d) $CD45^+CD3^+CD4^+IL\text{-}17^+$ T cells in the spleen T cells of different experimental groups were detected by flow cytometry. (e) The protein of CIA mouse joint synovium was extracted, and the expression of pro-inflammatory cytokines, including IL-*β*, IL-6, and TNF-*α*, in each group of mice was detected by Western blot. The Western blot data of each pro-inflammatory cytokine were quantitatively analyzed by ImageJ software. N.S., not significant; *$P < 0.05$, **$P < 0.01$, and ***$P < 0.001$.

bone volume percentage (BV/TV) (Figure 3e) was also performed by micro-CT, which objectively indicated that FA−PEG−R−NPs@siERN1 can effectively prevent bone loss. It is worth noting that there was no significant difference in the BMD and BV/TV index between the FA−PEG−R−NPs@siERN1 group and the FA−PEG−NPs@siERN1 group. The contradiction between the above data may be attributed to the fact that bone loss usually occurs in the later stages of disease development. Although FA−PEG−NPs@siERN1 does not have the best therapeutic effect, it slows disease progression to a large extent. Therefore, it is reasonable that the FA−PEG−NPs@siERN1 group did not exhibit serious bone loss. In addition, the swelling suppression and cartilage protection effects of the FA−PEG−NPs@siERN1 were detected by

https://doi.org/10.1021/acsnano.1c03726
ACS Nano XXXX, XXX, XXX−XXX

magnetic resonance imaging (MRI) (Figure 3b). The T2-weighted image shows that FA−PEG−NPs@siERN1 significantly reduces the degree of tissue and bone marrow edema and protects the articular cartilage from erosion.

The degree of inflammatory synovial tissue infiltration and articular cartilage damage can be objectively evaluated by hematoxylin and eosin (HE) staining. As shown in Figure 3c, the most serious hypertrophy and hyperplasia of the synovial lining cell layer were observed in the control group and R−NPs@siERN1 group, accompanied by a significant amount of inflammatory infiltration. Strong synovial stroma activation was observed, which was manifested by high cellularity with a dense distribution of fibroblasts and endothelial cells and abundant giant cells. No significant differences in the inflammatory damage of the synovial membrane and articular cartilage were observed between the two groups. A significant amount of synovial hyperplasia invaded the joint cavity and infiltrated the articular cartilage deep into the subchondral bone, causing full-thickness joint damage. Although the PEG−R−NPs@siERN1 group had slightly less inflammatory infiltration and cartilage destruction than the first two groups, significant synovial lining cell layer hypertrophy was observed, and the cartilage damage was also quite serious. Consistent with the treatment effect data, the FA−PEG−R−NPs@siERN1 group demonstrated the best inflammation control and cartilage protection effects. In the FA−PEG−R−NPs@siERN1 group, the siERN1 preparation effectively inhibited the intrusion of the hypertrophic synovial lining cell layer into the joint cavity and protected the integrity of the meniscus and articular cartilage. Although the FA−PEG−NPs@siERN1 group also controlled the hypertrophy and proliferation of the synovial lining cell layer and reduced its infiltration into the joint cavity to a certain extent, more serious cartilage damage was observed in comparison to the FA−PEG−R−NPs@siERN1 group. In addition, HE staining was scored objectively according to the Histological Synovitis Score (HSS) and the Modified Osteoarthritis Research Society International (OARSI) scoring standards (Supplementary Tables 3 and 4). In addition, the effects of FA−PEG−R−NPs@siERN1 on the inflammation control and chondroprotection in the CIA model were further evaluated (Figure 3f and g).

These data suggest that FA−PEG−R−NPs@siERN1 has the best therapeutic effect on the CIA models. FA−PEG−R−NPs@siERN1 can efficiently control local inflammation in the joints and effectively protects the articular cartilage and subchondral bone from inflammatory damage.

Role of FA−PEG−R−NPs@siERN1 during Immunomodulation and Inflammation Control in the CIA Model. T lymphocytes play an important role in immune regulation and are the executive cells of cell-mediated immunity. The ratio of the $CD45^+CD3^+CD4^+$ T cells to $CD45^+CD3^+CD8^+$ T cells is an important reference value for evaluating the body's immune status.[34−36] This ratio in the lymph nodes was calculated by performing flow cytometry (Figure 4a and Supplementary Figure 13a). The results showed that FA−PEG−R−NPs@siERN1 successfully regulated the systemic immune status of the CIA mice and inhibited the excessive activation of immune regulation. Notably, although not as good as FA−PEG−R−NPs@siERN1, FA−PEG−NPs@siERN1 still has a good immune regulation ability in the CIA mice. In addition, we collected splenic T cells for the same test and obtained experimental conclusions that are consistent with those for the lymph node T cells (Figure 4b and Supplementary Figure 13b).

Previous studies have confirmed that the imbalance between the T helper 17 (Th17) and T regulatory (Treg) cells plays an important role in the occurrence and development of autoimmune diseases.[37−40] Th17 cells are a pro-inflammatory subgroup that can promote autoimmunity and tissue damage. In contrast, Treg cells have immunosuppressive effects and can suppress autoimmunity. The proportions of the $CD45^+CD3^+CD4^+FoxP3^+$ Treg cells and $CD45^+CD3^+CD4^+IL\text{-}17^+$ Th17 cells were detected by flow cytometry (Figure 4c,d and Supplementary Figure 14). It was observed that FA−PEG−R−NPs@siERN1 upregulates the proportion of Treg cells and simultaneously downregulates the proportion of Th17 cells. FA−PEG−R−NPs@siERN1 promotes the balance between the Th17 and Treg cells to tilt toward Treg differentiation, which can help prevent excessive activation of the immune system.

The severity of inflammation in CIA is closely related to the immune status of the body. To this end, the level of local inflammation in the affected joint area of the CIA mice was detected by performing Western blotting and quantitative reverse transcription polymerase chain reaction (RT-qPCR). The expression of three pro-inflammatory cytokines, IL-1β, IL-6, and TNF-α, was detected (Figure 4e). Overall, the Western blot of the FA−PEG−R−NPs@siERN1 group had the lowest gray scale, indicating that FA−PEG−R−NPs@siERN1 significantly inhibits the expression of the above-mentioned three pro-inflammatory cytokines in the synovium of joint. The RT-qPCR data were consistent with the Western blot results, showing that FA−PEG−R−NPs@siERN1 simultaneously downregulated the mRNA levels of the three pro-inflammatory cytokines. In addition, the mRNA expression levels of three anti-inflammatory factors, including *Il-10*, *CD163*, and *CD206*, were evaluated. The results demonstrate that the mRNA levels of the three anti-inflammatory factors were upregulated in the FA−PEG−R−NPs@siERN1 group, indicating that the number of M2 macrophages increased, whereas the proportion of M1 macrophages decreased (Supplementary Figure 15); this result further confirms the flow cytometry data. Therefore, FA−PEG−R−NPs@siERN1 can regulate the body's immune state to restore homeostasis and inhibit inflammation.

Furthermore, immunofluorescence analysis was performed to visually observe the expression and distribution of pro-inflammatory cytokines in the local joints (Supplementary Figures 16−18). The data revealed that pro-inflammatory cytokines were mainly expressed in the hyperplastic synovial tissue, and a small amount was distributed in the articular cartilage and subchondral bone. Compared with other treatments, FA−PEG−R−NPs@siERN1 significantly inhibited the expression of pro-inflammatory cytokines. In addition, we measured the concentration of the pro-inflammatory cytokines in the serum using enzyme-linked immunosorbent assay (ELISA) to assess the level of systemic inflammation. As shown in Supplementary Figure 19, consistent with the previous data, FA−PEG−R−NPs@siERN1 significantly downregulated the pro-inflammatory cytokine levels in the serum, representing the best inhibitory effect on inflammation. Based on the above data, it was determined that FA−PEG−R−NPs@siERN1 can regulate the body's immune state to restore balance, thus exerting a good inflammation inhibitory effect.

Therapeutic Effect of FA−PEG−R−NPs@siERN1 in the DSS-Induced IBD Model. IBD is a common autoimmune inflammatory disease. This study objectively evaluated the therapeutic effect of FA−PEG−R−NPs@siERN1 in the DSS-

https://doi.org/10.1021/acsnano.1c03726
ACS Nano XXXX, XXX, XXX−XXX

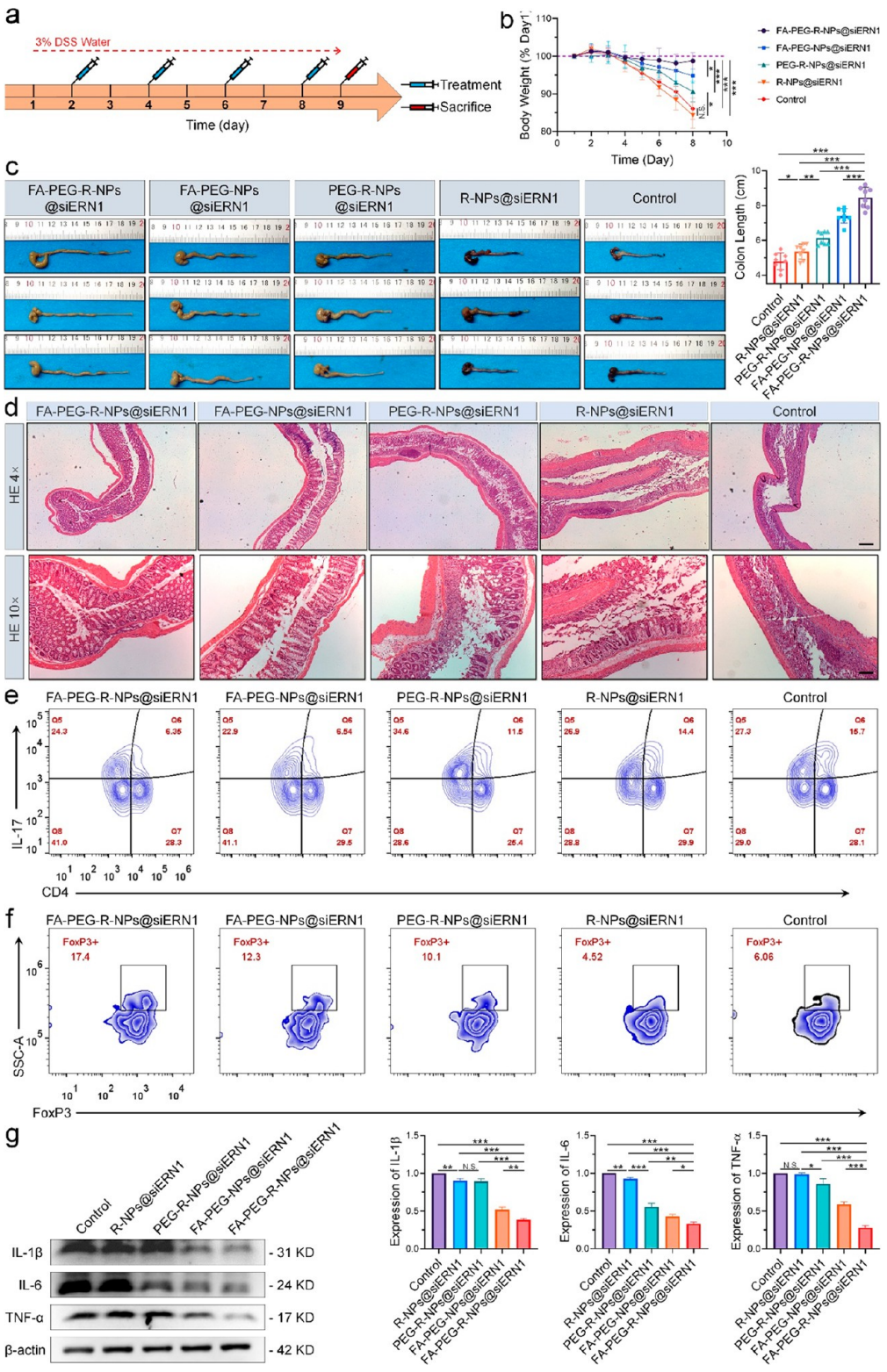

Figure 5. Intestinal protection and inflammation inhibitory effect of FA−PEG−R−NPs@siERN1 in a DSS-induced IBD model. (a) Schematic diagram of IBD model building and treatment schedule. (b) Changes in body weight of mice in each experimental group during treatment (N = 8). (c) On the third day after the last treatment, the mice were sacrificed, the mouse colon tissues were collected, and the colon lengths of the mice in each group were compared according to the ruler scale. (d) The histopathological section of the colon was stained with HE to observe the structural integrity of the colon, including goblet cells, villous structure, and muscle layer structure. The proportions of (e) $CD45^+CD3^+CD4^+IL\text{-}17^+$ Th17 cells and (f) $CD45^+CD3^+CD4^+CD25^+FoxP3^+$ Treg cells in the spleen T cells of different experimental groups were detected by flow cytometry. (g) The protein of IBD mouse colon was extracted, and the expression of pro-inflammatory cytokines, including IL-β, IL-6, and TNF-α, in each group of mice was detected by Western blot. The Western blot data of each pro-inflammatory cytokine were quantitatively analyzed by ImageJ software. N.S., not significant; *P < 0.05, **P < 0.01, and ***P < 0.001.

https://doi.org/10.1021/acsnano.1c03726
ACS Nano XXXX, XXX, XXX−XXX

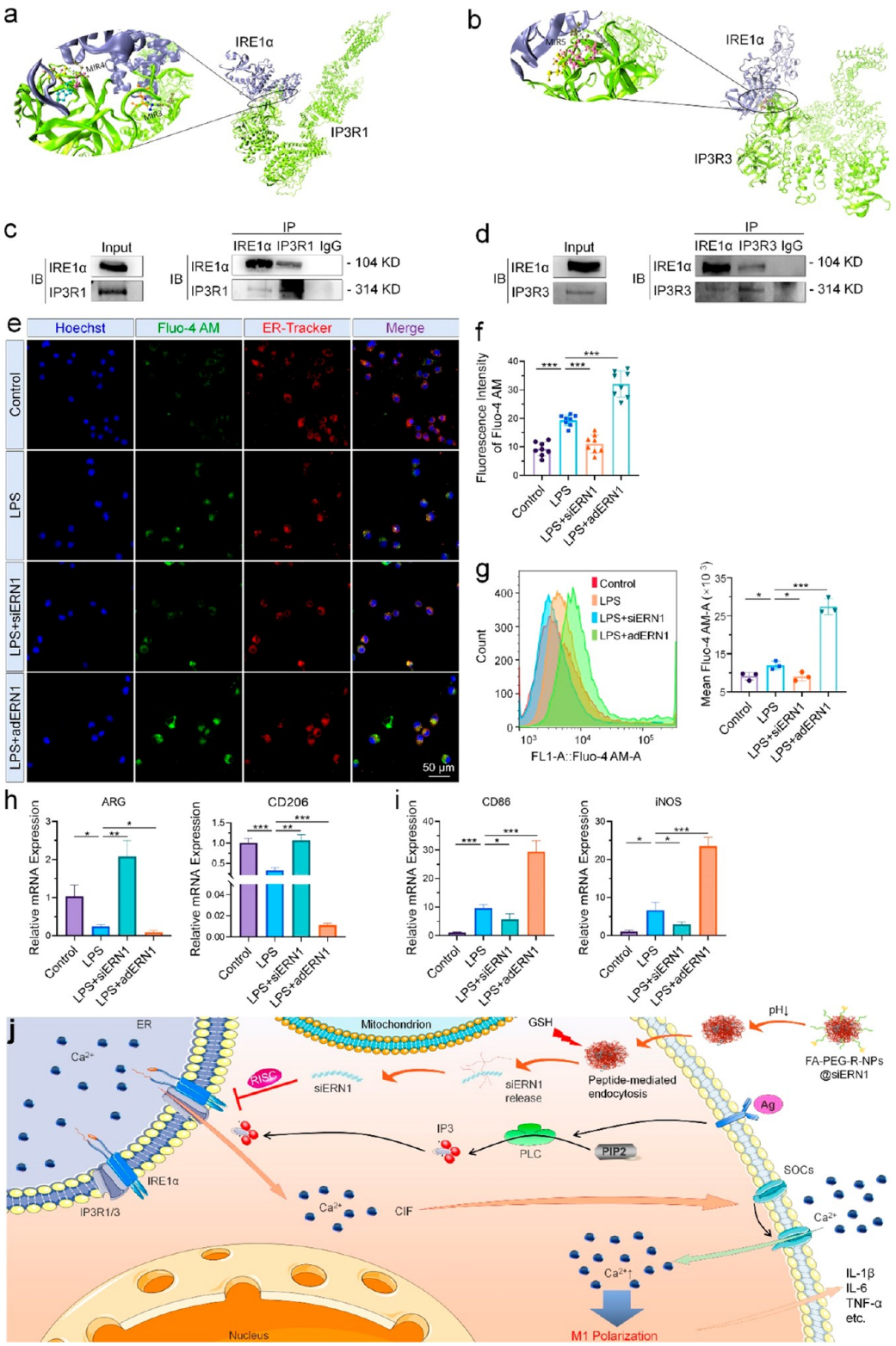

Figure 6. siERN1 promotes M2 polarization of macrophages by affecting the function of IP3R and regulating the intracellular Ca^{2+} concentration. The combination of IRE1*α* and (a) IP3R1 and (b) IP3R3 was simulated by Visual Molecular Dynamics technology. The co-immunoprecipitation technique once again proved the binding of IRE1*α* with (c) IP3R1 and (d) IP3R3. (e) Fluo-4 AM labels intracellular Ca^{2+} and shows the changes of Ca^{2+} concentration in LPS-induced M1 macrophages after knocking down or overexpressing ERN1 by fluorescence colocalization, RAW 264.7 cells without LPS stimulation as control, and (f) semiquantitative analysis of fluorescence intensity was performed by ImageJ software. (g) The changes of Ca^{2+} concentration of knockdown or overexpression of ERN1 in M1 macrophages induced by LPS were detected by flow cytometry. (h) The M2 and (i) M1 marker expression level of knockdown or overexpression of ERN1 in M1 macrophages induced by LPS was detected by RT-qPCR. (j) Schematic diagram of IRE1*α* binding to IP3R to regulate intracellular Ca^{2+} to promote M1 polarization of macrophages. N.S., not significant; *$P < 0.05$, **$P < 0.01$, and ***$P < 0.001$.

https://doi.org/10.1021/acsnano.1c03726
ACS Nano XXXX, XXX, XXX−XXX

induced IBD model to further verify its universal applicability. Similar to the CIA study, the targeting of FA−PEG−R−NPs@siERN1 was tested in IBD model animals (Supplementary Figure 20), and siERN1 preparations were grafted with FA, including FA−PEG−R−NPs@siERN1 and FA−PEG−NPs@siERN1, which also have superior targeting properties in the IBD model.

The IBD model was treated according to the design plan shown in Figure 5a. The entire treatment cycle required 9 days, in which the mice were continuously provided with drinking water containing 3% DSS. The preventive and therapeutic effects of the different siERN1 preparations on the IBD model were measured based on the daily weight changes. Figure 5b shows that the mice in each group began to lose weight on the third day of drinking the water containing 3% DSS. As the experiment continued, FA−PEG−R−NPs@siERN1 gradually controlled the weight loss of the mice, while the other groups of mice showed different degrees of weight loss. Among them, the weight loss of the mice in the R−NPs@siERN1 group and the control group was the most serious.

On the ninth day of drinking the DSS water, the mice were sacrificed, and the colon from the anus to the ileocecal area was collected. The length of the colon, which can directly reflect the severity of IBD, was analyzed (Figure 5c). The colons of the mice in the R−NPs@siERN1 group and the control group appeared dark purple, and significant differences were observed between the colons of the mice in each group. Specifically, FA−PEG−R−NPs@siERN1 maintained the colon length of the IBD mice at approximately 8.2 cm (the average length of a normal colon is 9.0 cm, Supplementary Figure 21). Compared with the FA−PEG−R−NPs@siERN1 group, the FA−PEG−NPs@siERN1 group had a slightly worse effect on colon length (7.7 cm). As expected, the length of the colon of the mice in the R−NPs@siERN1 group and the control group was the shortest (5.1 and 4.9 cm, respectively), representing the worst disease control effect. Undoubtedly, FA−PEG−R−NPs@siERN1 can inhibit the intestinal symptoms and relieve inflammation and weight loss in the IBD mice. The colon tissues of the mice in each group were collected and stained for histopathological analysis (Figure 5d). In the FA−PEG−R−NPs@siERN1 group, relatively complete and normal intestinal structures, including dense goblet cells and crypt structures, were observed. Colon ulcers or noticeable inflammatory cell infiltration was not observed in any layer of the intestine. However, intestinal injuries, including necrosis and colon ulcers, were observed in the intestinal tissue of the other four groups.

As shown in Figure 5e and f, the proportion of $CD45^+CD3^+CD4^+IL\text{-}17^+$ T lymphocytes in the FA−PEG−R−NPs@siERN1-treated mice was 6.35%, and the proportion of $CD45^+CD3^+CD4^+FoxP3^+$ T lymphocytes was 17.4%. In the other groups, the proportion of Th17 cells increased and the proportion of Treg cells decreased to varying degrees, indicating that FA−PEG−R−NPs@siERN1 can promote T cell differentiate into Treg cells, reduce the proportion of Th17 cells, and promote the body's immune state to restore balance.

The levels of the different pro-inflammatory cytokines, including IL-1β, IL-6, and TNF-α, in the colon tissue were detected through Western blotting analysis (Figure 5g). Quantitative analysis showed that levels of the three pro-inflammatory cytokines were reduced in the colon tissue of the FA−PEG−R−NPs@siERN1-treated mice compared to that of the control group. Similarly, RT-qPCR was used to detect the mRNA levels of the pro-inflammatory and anti-inflammatory cytokines in the affected colon tissue (Supplementary Figure 22), and the results were found to be consistent with the previous CIA model data. FA−PEG−R−NPs@siERN1 not only inhibited the expression of the pro-inflammatory cytokines but also upregulated the expression of the anti-inflammatory cytokines. The results also showed that the proportion of M2 macrophages in the FA−PEG−R−NPs@siERN1 treatment group increased, whereas the number of M1 macrophages decreased, indicating that FA−PEG−R−NPs@siERN1 promoted the polarization of the M2 macrophages, thereby regulating the body's return to homeostasis.

Similarly, the immunofluorescence assay showed that FA−PEG−R−NPs@siERN1 can effectively inhibit the expression of several pro-inflammatory cytokines in the affected colon tissue while protecting the normal structure of the colon tissue, suggesting that it has a superior disease treatment effect (Supplementary Figures 23−25). The ELISA results showed that FA−PEG−R−NPs@siERN1 can control the local inflammation of the intestine and regulate systemic inflammation (Supplementary Figure 26).

Therefore, FA−PEG−R−NPs@siERN1 can alleviate IBD progression in mice by regulating the immune state, controlling weight loss, protecting the normal structure of the mouse colon, and reducing the level of local and systemic inflammation.

Mechanism of siERN1 in Restoring Immune Homeostasis and Alleviating Inflammation. IRE1α is an ER transmembrane sensor. Previous studies have confirmed that IRE1α is related to the function and secretion pathway of the ER. Recent studies have shown that one of the noncanonical functions of IRE1α is associated with the IP3R and that it regulates calcium signal transduction by controlling the intracellular Ca^{2+} concentration and various cellular metabolic activities.[41−43] In this study, by using visual molecular dynamics (VMD) technology, IRE1α was predicted to interact with the two subtypes of IP3R, namely, IP3R1 and IP3R3 (Figure 6a and b). Subsequently, a co-immunoprecipitation assay was performed to further verify the protein interconnection between IRE1α and IP3R1/3. The co-immunoprecipitation data are consistent with the VMD results, which indicate that an interaction occurs between IRE1α and IP3R1/3 (Figure 6c and d). We further explored the relationship between the effect of *ERN1* and the intracellular Ca^{2+} concentration under inflammatory conditions. The fluorescence intensity and flow cytometry data (Figure 6e−g) show that the Ca^{2+} concentration increased in the LPS-induced M1 macrophages. The overexpression of *ERN1* increases the intracellular Ca^{2+} concentration, whereas knockdown of ERN1 through siRNA reduces that concentration under LPS treatment conditions.

Previous studies have reported that the Ca^{2+} concentration in macrophages affects the regulation of macrophage polarization.[44,45] Based on the above data, the polarization direction of the macrophages was further detected by RT-qPCR (Figure 6h and i). As expected, after *ERN1* knockdown, the mRNA expression of the M2 macrophage markers, including *Arg* and *CD206*, was upregulated, whereas the mRNA expression of the M1 macrophage markers *CD86* and *iNOS* was downregulated. The results confirm that the siERN1-nanoprodrug reduces the role of ERN1 and its interaction with IP3R1/3 by downregulating its expression, prevents Ca^{2+} from entering the cytoplasm through ER, and further interferes with the intracellular Ca^{2+} concentration, thereby inhibiting the M1 polarization and promoting M2 polarization of macrophages (Figure 6j). In the RA and IBD mouse models, the siERN1-

https://doi.org/10.1021/acsnano.1c03726
ACS Nano XXXX, XXX, XXX−XXX

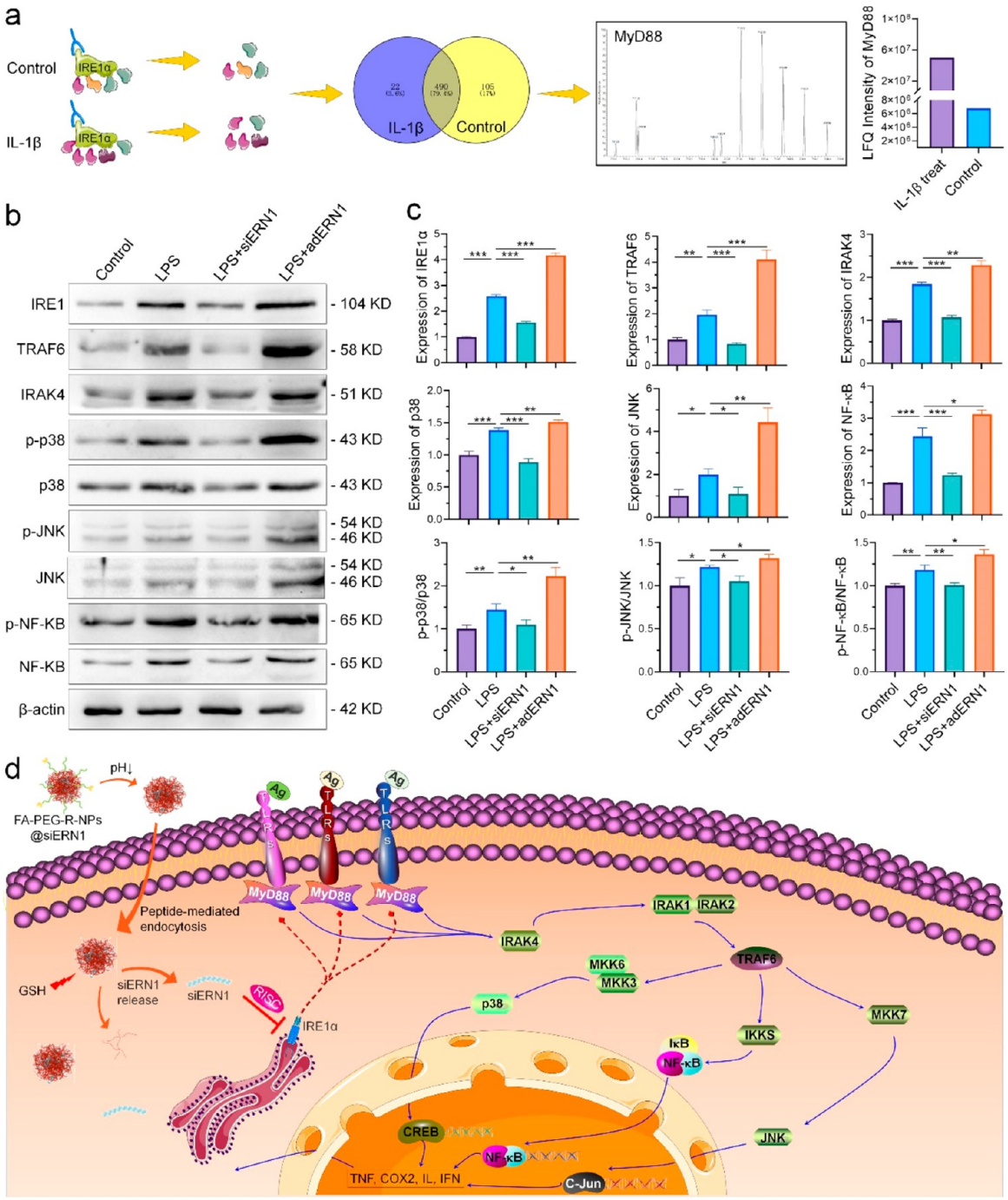

Figure 7. siERN1 inhibits inflammation by blocking the MyD88-dependent TLR signaling pathway. (a) Scheme of the method used to identify potential molecules involved in ERN1-mediated regulation of IL-1*β*-induced inflammation by label-free quantitative proteomics analysis, such as ERN1-associated proteins in IL-1*β*-treated inflammation. Immunoprecipitation was performed with myc antibody from both pcDNA3.1(−)myc−ERN1 transfected macrophage with or without IL1-*β*, followed by high-sensitivity mass spectrometry. (b) Western blot was used to detect the expression of key proteins in the TLR signaling pathway in the LPS-induced BMDM M1 polarization model after knocking down or overexpressing ERN1. (c) Semiquantitative analysis of IRE1*α*, TRAF6, IRAK4, JNK, p38, and NF-*κ*B expression in each treatment group in Western blot data was performed by ImageJ software. The phosphorylation levels of JNK, p38, and NF-*κ*B were further calculated. (d) Schematic diagram of ERN1 regulating cell pro-inflammatory cytokine expression through the MyD88-dependent TLR signaling pathway. *$P < 0.05$, **$P < 0.01$, and ***$P < 0.001$.

nanoprodrug promoted the polarization of M2 macrophages and the secretion of anti-inflammatory factors such as IL-10, CD163, and CD206. These factors are crucial for the Treg cell-mediated control of immunosuppressive effects and participate in suppressing autoimmunity *in vivo*. The activated macrophages can profoundly affect the phenotype and function of Treg cells, and the expression level of FoxP3 notably affects the maintenance of immune homeostasis.[38,46−48]

In order to determine the molecules that are involved in the IRE1*α*-mediated regulation of inflammation, the label-free quantitative proteomics assay was performed to detect the IRE1*α*-enriched proteins (Supplementary Schemes 2 and 3).

https://doi.org/10.1021/acsnano.1c03726
ACS Nano XXXX, XXX, XXX−XXX

Compared with the 617 hits from the pcDNA3.1(−)myc-*ERN1*-transfected macrophages with or without the IL-1β treatment, 22 hits with and 105 hits without the IL-1β treatment were identified as IRE1α-associated proteins; these proteins showed significantly different enrichment during inflammation. The expression level of MyD88 was associated with *ERN1* and was significantly upregulated with the IL-1β treatment (Figure 7a). MyD88, which is a key linker molecule in the TLR signaling pathway, plays an important role in transmitting upstream information and disease occurrence and development. The TLR signaling pathway is reported to implicate synovitis and joint destruction in RA through controlling the production of inflammatory mediators. The data show that *siERN1* downregulates the expression of the MyD88-dependent TLR signaling pathway molecules, whereas overexpression of *ERN1* upregulates the expression of the same molecules in this pathway under LPS treatment conditions, including TRAF6, IRAK4, p-p38/p38, p-JNK/JNK, and p-NF-κB/NF-κB. It is suggested that IRE1α participates in the regulation of the MyD88-dependent TLR signaling pathway, indicating that it plays an important role in inflammatory diseases (Figure 7b and c). Intense efforts have been invested to prove that FA−PEG−R−NPs@siERN1 acts as a regulator of macrophage polarization and blocks the MyD88-dependent TLR signaling pathway (Figure 7d). Furthermore, our result revealed that the siERN1-nanoprodrug will not cause an increase in susceptibility to bacterial infection in CIA mice (Supplementary Figure 27).[49]

Taken together, the siERN1-nanoprodrug, which can control disease in CIA mice, maintained the normal immune state by promoting the polarization of M2 macrophages to secrete anti-inflammatory cytokines, interaction between macrophages and T cells, upregulation of FoxP3, and the homeostasis of Treg/Th cells. Although the effect of the nanoprodrug in mice cannot be equivalent to that in humans, the siERN1-nanoprodrug can be used as a reliable drug delivery method for clinical applications in the future.

CONCLUSION

This study confirms that the siERN1-nanoprodrug can modulate the polarization of the macrophages by regulating the Ca^{2+} concentration and serves as an antagonist for MyD88-dependent TLR signaling, providing a promising approach to suppress this basic inflammatory pathway and treat various TLR-associated diseases, including autoimmune inflammatory diseases. Moreover, this study verifies that *ERN1* is an effective target for autoimmune inflammatory diseases, thus providing hopeful insights into the understanding of the siERN1 drug and its underlying mechanisms. Our research lays a solid foundation for further development of siERN1 drugs. The construction and identification of siERN1 drugs may expand the application of innovative nanomedicines and gene therapy in various pathologies and diseases.

METHODS

Human Subjects. All biomedical studies involving humans in this study were reviewed and approved by the Ethics Committee of Chongqing Medical University, and full written consents were obtained before the operative procedure. In this study, 23 clinical samples were collected, and a total of 14 samples of protein were collected for Western blot, including 5 OA samples, 5 RA samples, and 4 normal cartilage tissue. All samples were snap-frozen and stored in liquid nitrogen for a long time.

Cell Lines. HEK 293 cells, RAW 264.7 cells, and THP-1 cells were purchased from the Cell Bank of the Chinese Academy of Sciences (Shanghai, China). All cells were routinely checked every two months for mycoplasma contamination using the EZ-PCR mycoplasma test kit (Biological Industries) according to the manufacturer's protocol. HEK 293 cells were cultured in Dulbecco's modified Eagle medium (DMEM) containing 10% fetal bovine serum (FBS) and 50.0 μg/mL penicillin−streptomycin. RAW 264.7 cells were cultured in Dulbecco's modified Eagle medium alpha (α-MEM) containing 10% FBS and 50.0 μg/mL penicillin−streptomycin. THP-1 cells were cultured in RPMI 1640 containing 10% FBS and 50.0 μg/mL penicillin−streptomycin. All cells were cultured at 37 °C in a humidified incubator with 5% CO_2.

Design and Synthesis of siERN1. Three siRNAs of ERN1 were designed and synthesized by Sangon Biotech (Shanghai) Co., Ltd. The specific siRNA sequence is shown in Supplementary Table 1. HEK 293 cells were seeded in six-well plates at a density of 60−70%. After the cells adhered overnight, different siRNAs were added at a working concentration of 50.0 nM, and PEI was used as a transfection reagent. siRNA and cells were incubated for 8 h, and the medium was removed and replaced with a new DMEM containing 10% FBS and 1% penicillin−streptomycin. The total RNA was collected for RT-qPCR testing at 24 h, and the total cell protein was collected for Western blot at 48 h.

Role of ERN1 in LPS-Induced M1 Polarization of RAW 264.7 Cells and THP-1 Cells. RAW 264.7 cells were seeded in a six-well plate at a density of 70%. After the cells adhered, ERN1 overexpressing adenovirus (adERN1) or siERN1 was added. After transfection for 8 h, the original medium was removed and replaced with α-MEM containing 10% FBS. After culturing for 24 h, RNA was collected for RT-qPCR, or for 48 h, total protein was collected for Western blot detection.

THP-1 cells were seeded in a six-well plate at a density of about 80%, and 100.0 ng/mL phorbol 12-myristate 13-acetate (PMA) was induced for 24 h to promote their adherence. After treatment with siERN1 or AdERN1 according to the previous method (transfection reagent is Lipo2000) for 6 h, the original medium was removed and 1640 medium containing 1.0 μg/mL LPS, 10% FBS, and 1% penicillin−streptomycin was added. After incubation for another 24 h, RNA was collected for RT-qPCR detection.

Synthesis and Characterization of FA−PEG−R−NPs@siERN1. Under the protection of nitrogen, 0.109 g of 2-aminoethanol and 0.520 g of *N*,*N*′-(dithiodi-2,1-ethanediyl)bis(acrylamide) (n/n = 0.9) were added to 5.0 mL of a 25% methanol aqueous solution. The reaction mixture was stirred fully at 60 °C in the dark for 48 h to obtain the product, poly(β-amino amine) containing disulfide bonds (ss-PBAA). A 0.276 g amount of PEI was dissolved in 2.0 mL of 25% methanol aqueous solution and then added to the previously obtained ss-PBAA solution to prepare ss-PBAA-PEI. In detail, the molar ratio of primary amine in PEI to reactive groups in ss-PBAA was 4:1, and the reaction was continued for another 24 h under nitrogen protection at 45 °C. Then the above solution was diluted to 30.0 mL with water and acidified to pH = 4 with 6 M hydrochloric acid. Then the solution was transferred to a dialysis bag (MWCO = 8000 Da) for dialysis for 2 days to remove unreacted reactants. Finally, the solution was freeze-dried for 2 days to obtain ss-PBAA−PEI.

The ss-PBAA−PEI was dissolved in an aqueous sodium chloride solution of pH = 8.0, and the penetrating peptide was added to the above solution, vortexed for 5 s, and incubated at 37 °C for 30 min. Then siERN1 was put into the above solution and diluted to 2.0 mL with sodium chloride solution, vortexed for 5 s, and incubated at 37 °C for another 30 min. Finally, the product R−ss-PBAA−PEI@siERN1 was obtained.

The pH of the R−ss-PBAA−PEI@siERN1 solution was adjusted to 8.0 with 0.3 M sodium hydroxide solution; then an appropriate amount of CHO−PEG_{2000}−COOH (m/m = 2:1) was added. After incubating for 12 h at 37 °C, dialysis was continued for 2 days according to the previous method, and the unreacted reactants were removed to obtain the COOH−PEG−R−ss-PBAA−PEI@siERN1 solution. Subsequently, the above-mentioned complex solution was added to EDC and NHS in a molar ratio of 1:5, and after activation at room

https://doi.org/10.1021/acsnano.1c03726
ACS Nano XXXX, XXX, XXX−XXX

temperature for 25 min, the unreacted EDC and NHS were removed by ultrafiltration. Then excess folic acid was added, and the mixture incubated for 6 h at room temperature to remove unreacted FA again by ultrafiltration to obtain the final product, FA−PEG−R−NPs@siERN1.

After the nanoprodrug assembly was completed, the Nano-300 ultra-micro nucleic acid detector (Shanghai Jiapeng Technology Co., Ltd.) was used to measure the concentration of siERN1 in different preparations. The appearance and size of the nanoprodrug was observed by TEM, and the hydrodynamic size of the nanoprodrug was measured by DLS.

***In Vitro* Release.** A 5.0 mg amount of FA−PEG−R−NPs@siRNA was weighed and placed in a dialysis bag (MWCO = 18 000 Da) at a concentration of 1.0 mg/mL. In order to observe the release behavior of the nanomedicine under different conditions, the dialysate was set to three types: pH = 7.4, pH = 6.0, and pH = 6.0 with GSH solution at 37 °C, with 100 rmp/min continuous shaking. A 1.0 mL amount of the released solution was collected outside the dialysis bag at a predetermined time point, and the same volume of medium was added to the dialysis bag at the same time. Finally, the release of siERN1 was measured, and the release rate of the nanoprodrug under different conditions was calculated.

MTT Assay. After centrifugation, RAW 264.7 cells were resuspended in α-MEM containing 10% FBS and 1% penicillin−streptomycin and counted to make a suspension with a cell density of 5×10^5/mL; 200.0 μL (about 1×10^5 cells) was inoculated per well in a 96-well plate. After the cells adhered overnight, the original medium was removed and 100.0 μL of each siERN1 preparation was added to a 96-well plate according to the multiple dilution method (siERN1 concentration range 3.13−400.0 μg/mL). Serum-free α-MEM was used as the control group. After 24 h of cocultivation, 10.0 μL of 5.0 mg/mL MTT reagent was added to each well, and the co-incubation was continued for another 4 h. The medium was aspirated in each well carefully, and 150.0 μL of dimethyl sulfoxide was added to each well and placed on a shaker to shake at low speed for 10 min to fully dissolve the crystals. Finally, the absorbance of each well was measured at 490 nm by the microplate reader. The cell viability was calculated using eq 1.

$$\text{Cell viability (\%)} = \frac{A_{\text{sample}}}{A_{\text{control}}} \times 100\% \quad (1)$$

In eq 1, A_{sample} and A_{control} were denoted as the absorbencies of the sample and control, respectively.

Hemocompatibility. The hemocompatibility levels of the siERN1 preparation were determined according to the established standard: ISO 10993-4. Rabbits were purchased from the Laboratory Animal Center of Chongqing Medical University. Briefly, after the rabbits were anesthetized with 1% sodium pentobarbital, 10.0 mL of fresh blood was collected. The blood was transferred to a 15.0 mL beaker and stirred with a cotton swab to remove fibrinogen. A 15.0 mL amount of physiological saline was added, and the mixture was transferred to a 50.0 mL centrifuge tube, shaken well, and centrifuged; the supernatant was then poured out. This was repeated 3 or 4 times until there was no blood in the supernatant. Then the appropriate amount of red blood cells (RBCs) was extracted, and normal saline was added to make a 2% (v/v) cell suspension. A 2.0 mL amount of cell suspension was withdrawn and transferred to a 4.0 mL EP tube, along with 100.0 or 300.0 μL of different siERN1 preparations, into an EP tube, respectively, mixed by vortexing, and then incubated at 37 °C in a thermostatic water bath for 3 h. PBS and Triton X-100 (1×10^4 mg mL^{-1}, a surfactant known to lyse RBCs) were used as negative and positive controls, respectively. Then, RBCs were centrifuged at 3000 rpm for 10 min, and then 100.0 mL of the supernatant of each sample was transferred to a 96-well plate. The free hemoglobin in the supernatant was measured with a Bio-Rad 680 microplate reader at 490 nm. The hemolysis ratio of RBCs was calculated using eq 2.

$$\text{Hemolytic ratio (\%)} = \frac{A_{\text{sample}} - A_{\text{negative control}}}{A_{\text{positive control}} - A_{\text{negative control}}} \times 100\% \quad (2)$$

In eq 2, A_{sample}, $A_{\text{negitive control}}$, and $A_{\text{positive control}}$ were denoted as the absorbencies of sample and negative and positive controls, respectively.

Cell Uptake. The RAW264.7 cells were cultured for 12 h in an incubator in DMEM at 37 °C and were then activated by LPS for 6 h. Then, the cy5-labeled siERN1 formulation solution in DMEM was used to refresh the media. The equivalent dose of siERN1 in DMEM is 2.0 mg/mL and was co-incubated with cells for an additional 1 or 2 h. After washing the cells on a glass coverslip, they were fixed with 4% (w/v) PBS-buffered formaldehyde for half an hour. Next, 4′,6-diamidino-2-phenylindole dihydrochloride (DAPI) was used to stain the nuclei for 3 min. Finally, cell uptake imaging was performed by CLSM. The fluorescence intensity was analyzed semiquantitatively with the help of ImageJ software.

Pharmacokinetics. The SD rat CIA model was constructed by intradermal injection of the induction reagent on the back. Then the cy5-labeled siERN1 preparations were injected through the tail vein. A 250.0 μL amount of blood was collected through the orbit at a predetermined time point (including 15 min, 30 min, 1 h, 2 h, 4 h, 6 h, 8 h, 12 h, and 24 h), and heparin 10 UI was added for anticoagulation. The plasma was collected by centrifugation at 5000 rpm for 5 min. After all the samples were collected, each group of samples was added to a 96-well plate according to the time point, with 100.0 μL of plasma per well. The fluorescence intensity in the plasma was detected with the aid of a fluorescence detection system. Subsequently, the fluorescence intensity was semiquantitatively analyzed by ImageJ software to reflect the change trend of siERN1 drug concentration in plasma over time.

CIA Model and DSS-Induced IBD Model. All the animal experiments were approved by Chongqing Medical University Institutional Animal Care and Use Committee. Mice were group housed (25 °C) with a 12:12 h light−dark cyclephotoperiod, and allowed unrestricted access to potables and standard mouse chow.

The modeling method of CIA is as described in the previous work.[50] Immunization grade bovine type II collagen (CII) and Freund's complete adjuvant (FCA) were mixed and emulsified in an ice box at a ratio of 1:1. The emulsified drug was injected intracutaneously at the base of the tail of DBA/1J mice for the primary immunization of the CIA model. A booster immunization was performed on the 21st day after the primary immunization. Booster immunization is an emulsification with CII and FIA, and the details of the method are the same as the primary immunization. The sign of successful modeling of CIA is redness and swelling of joints in the limbs of mice.

The IBD model was induced in 6−8-week-old C57BL/6J male mice through replacing their drinking water with a 3% (wt/v) DSS solution for 9 days. The daily mental state and general condition of the mice were observed actively during the experiment.

***In Vivo* Biodistribution of FA−PEG−R−NPs@siERN1 in CIA Models and IBD Models.** Each siERN1 preparation was labeled with ICG. After the mouse model was successfully established, a therapeutic dose of ICG-nanoprodrugs was injected through the tail vein. At 12 h after drug injection, the fluorescence distribution in the mice was observed by *in vivo* imaging technology. The excitation wavelength and emission wavelength of ICG are 730 and 830 nm, respectively.

A therapeutic dose of the cy5-labeled siERN1 nanoprodrugs was injected through the tail vein, including FA−PEG−R−NPs@cy5-siERN, FA−PEG−NPs@cy5-siERN1, PEG−R−NPs@cy5-siERN1, and R−NPs@cy5-siERN1. Six hours after the injection of the drug, the mice in each group were sacrificed and samples were collected, including the heart, liver, spleen, lung, kidney, and limbs. The fluorescence imaging system was used to detect the distribution of the drug in the organs. The fluorescence intensity was analyzed semiquantitatively with the help of ImageJ software.

***In Vivo* RA Therapy and IBD Therapy.** The first treatment of CIA mice was performed with booster immunization by intravenous administration. For four kinds of siERN1 conjugates, the equivalent dose of siERN1 was 2.0 mg per kg body weight (mg (kg BW)$^{-1}$). Subsequently, the drug was administered every 3 days for a total of 9 times. The mice were euthanized on the third day after the last treatment, and tissue samples such as blood, joints, lymph nodes, and spleen were collected for subsequent testing. During the entire

https://doi.org/10.1021/acsnano.1c03726
ACS Nano XXXX, XXX, XXX−XXX

treatment period, the mice were subjected to arthritis score determination every 3 days.

The mice were continuously fed sterile drinking water containing 3% DSS according to the above method. The first administration of DSS drinking water was recorded as the first day of the experiment. The first treatment was given on the second day of the experiment, a total of 4 times. For four types of siERN1 conjugates, the equivalent dose of siERN1 was 2.0 mg (kg BW)$^{-1}$. During the experiment, the mice were weighed daily, and the characteristics and color of the mouse feces were observed. The mice were sacrificed on the ninth day of the experiment, and tissue samples were collected, including colon, blood, lymph nodes, and spleen. At the same time, a ruler was used to measure the length of the colon and pictures were taken.

Micro-CT and Magnetic Resonance Imaging. The mice were sacrificed on the third day after the last treatment, and samples of both hind limbs were collected. Subsequently, the samples were fixed on the holder, scanned, and three-dimensionally reconstructed with the aid of a micro-CT system (vivaCT40, SCANCO Medical AG, Switzerland). At the same time, the bone density and bone mass of the foot in the hind paw were measured by micro-CT. Three samples were randomly selected for each group. Then MRI scans were performed by an MRI system (Biospec 70/20USR, Bruker, Germany) to evaluate the swelling of the soft tissues and cartilage damage of the hind limbs of the mice.

Hematoxylin−Eosin Staining and Immunofluorescence Assay. All the experimental mice were sacrificed, and the knee joints were obtained at 48 days after the primary immunization. Then, all the samples were fixed using 4% (w/v) PBS-buffered paraformaldehyde overnight and placed in 15% (w/v) EDTA solution for decalcification. Twenty-one days later, all the samples were washed, embedded in paraffin, and sliced for histopathological and immunofluorescence analyses. The knee joint sections were stained with HE to observe the morphology of the joint and the distribution of inflammatory cytokines. The histopathological alterations were detected by microscope. The histopathological alterations of the knee joints were detected by microscope (Nikon Eclipse Ti, Optical Apparatus Co., Ardmore, USA). In addition, semiquantitative analyses of the proinflammatory cytokines were performed by ImageJ software through measurement of the relative positive areas.

Flow Cytometry. The mice were sacrificed on the third day after the last treatment; then the spleens and lymph nodes were separated and T lymphocytes extracted. The extracted spleen and lymph node T cells were stained for flow cytometry, and the T cell classification was analyzed by different antibody staining, such as FITC anti-mouse CD3, APC anti-mouse CD4, Brilliant Violet 510 anti-mouse CD8a, APC/Cyanine7 anti-mouse CD45, Brilliant Violet 421 anti-mouse CD25, Brilliant Violet 421 anti-mouse IL-17A, and PE anti-mouse FOXP3.

Transfection of RAW 2647.4 Cells with Plasmids and Collection of Samples for Mass Spectrum Analysis. The RAW 264.7 cells were plated and transfected with the plasmid pcDNA3.1(−)-Myc-*ERN1* with or without IL-1β treatment. Forty-eight hours later, 400.0 μL of IP buffer was added, the cells were lysed on ice for 30 min and centrifuged at 15 000 rpm and 4 °C for 15 min, the supernatant was collected, Anti-Myc antibody was added, and the mixture was incubated overnight on a 4 °C rotary mixer. The protein G magnetic beads were washed three times with precooled IP buffer, and 200.0 μL of PBS was added to resuspend the beads after washing five times; then the beads were collected and analyzed for the label-free quantitative proteomics assay to determine the IRE1α-enriched proteins (Shanghai Bioprofile Technology Co., Ltd., Shanghai, China).

Co-immunoprecipitation. HEK 293 cells were seeded in a 15.0 cm dish. After the cell density reached 95%, the original medium was removed and the dish was washed three times with precooled PBS. Subsequently, 1.0 mL of IP buffer containing phenylmethylsulfonyl fluoride was added, and the cells were lysed on ice for 30 min. The lysate was transferred to a 1.5 mL EP tube and centrifuged at 15 000 rpm at 4 °C for 15 min, and the supernatant was collected for subsequent experiments. The collected supernatant was divided into four parts, set as input group, IgG group, IRE1α group, and IP3R1 or IP3R3 group. The corresponding antibodies were added respectively and were placed on a rotator and rotated overnight at 4 °C. The beads were washed three times using IP buffer; they were then added to the above groups and continued to rotate at 4 °C for another 2 h. The beads were collected and washed again with IP buffer three times. Finally, 50.0 μL of SDS was added to resuspend the beads, which were boiled to collect the protein. Western blot was used to detect the presence of proteins in each group to verify the binding of IP3R and IRE1α.

Fluorescence Labeling of Intracellular Ca^{2+} and Quantification of Ca^{2+} Concentration by Flow Cytometry. RAW 264.7 cells were seeded and transfected with siERN1 or adERN1 according to the above method, including four groups (control, LPS, LPS+adERN1, and LPS+siERN1). The cells were stained after 24 h of cocultivation with 1.0 μg/mL of LPS. First, ER-Tracker red (1.0 μM) and Fluo-4 AM (4.0 μM) were diluted in Hanks' balanced salt solution (HBSS); then 400.0 μL of the above solution was added to each group to cover the cells and incubated at 37 °C for 30 min. After washing three times with HBSS, 1.0 mL of DMEM without FBS was added, and the mixture continued to incubate for another 30 min to ensure that Fluo-4 AM is transformed into Fluo-4 in the cells. Then an appropriate amount of Hoechst 33342 solution was added to cover the cells, and the cells were incubated at 37 °C for 30 min. Finally, after washing the cells with HBSS, DMEM containing 10% FBS was added to cover the cells, and the fluorescence was detected using a confocal laser scanning microscope. Then flow cytometry quantitative analysis of the same four groups of the above samples was performed.

Generation of Bone Marrow Derived Macrophages (BMDMs). After being sacrificed, the mice were soaked in 75% alcohol for 10 min; then bilateral hind limbs were removed and placed in conical tubes containing 5% FBS and 5% penicillin−fosfomycin DMEM medium. Then a 1.0 mL syringe was used to draw DMEM containing 10% FBS and penicillin−streptomycin to flush the bone marrow cavity until the backbone turns white. Then the bone marrow washing solution was transferred to a 15.0 mL centrifuge tube, and 5 times the volume of red blood cell lysate was add. After co-incubation for 10 min, the cells were centrifuged at 2000 rpm for 5 min. The supernatant was discarded, and the cells were resuspended in DMEM containing 10% FBS, 1% penicillin−streptomycin, and 50 ng/mL mouse M-CSF. The cells were placed in a cell culture dish and cultured for 4 days. The original medium was removed, and the same DMEM containing M-CSF was added again. After culturing for another 3 days, the original medium was removed, and the cells were washed with sterile PBS three times to wash away the nonadherent cells. The BMDMs were scraped gently with a cell scraper from the cell culture dish, and a single-cell suspension was prepared and counted for subsequent experiments.

TLR Signal Pathway Research. In order to explore the relevant mechanism of siERN1 inhibiting inflammation, a study was carried out in BMDMs. Consistent with the method described above for transfection of siERN1 or adER1N in RAW 264.7 cells, ERN1 was overexpressed or knocked down in BMDMs. Subsequently, 1.0 μg/mL LPS was added to the culture medium, and cell proteins were collected after 48 h of incubation. The expression of TLR signaling pathway related proteins was detected by Western blot.

Determination of the Number of Bacteria in Blood and Organs.[49] *Staphylococcus aureus* was inoculated on tryptic soy agar and cultured overnight at 37 °C, then selected monoclonal bacteria were inoculated into tryptic soy broth and incubated at 37 °C, 220 rpm, for 15 h. The bacteria were diluted with PBS, and the bacterial concentration was adjusted to 1×10^7 CFU/mL by spectrophotometer. The CIA model mice were constructed according to the method described above, and a therapeutic dose of siERN1 nanoprodrug was given on the 21st day; the treatment was performed every 2 days for a total of 5 times. Subsequently, 100.0 mL of prepared *S. aureus* solution was injected into the CIA model mice through the tail vein, and the mice in the control group were injected with normal saline, then given the same dose of *S. aureus* solution. The blood, spleen, and kidney of the mice were collected on the first, second, and fifth days, respectively. The spleen and kidney were dissected and homogenized in sterile water containing 0.5% Triton X-100. Subsequently, the spleen and kidney homogenate and blood were diluted 10 times, then inoculated on trypsin soy agar and cultured for 24 h to determine the bacterial CFUs.

https://doi.org/10.1021/acsnano.1c03726
ACS Nano XXXX, XXX, XXX−XXX

Western Blotting. Cells were washed on ice with precooled PBS, then lysed over 30 min with ice-cold RIPA lysis buffer containing a cocktail of protease inhibitors and phosphatase inhibitors with gentle agitation every 10 min. Cellular debris was clarified (15 000 rmp, 15 min, 4 °C). Sodium dodecyl sulfate was added to the supernatant and boiled at 95 °C for 10 min. Protein lysates were resolved on PAGE 8−12% Bis-Tris protein gels using running buffer, transferred to a polyvinylidene fluoride (PVDF) membrane, and blocked with 5% bovine serum albumin in PBS. They were incubated overnight with the primary antibody of the relevant target protein at 4 °C. The PVDF membrane was washed three times with Tris-buffered saline Tween (TBST) buffer, each for 10 min. Then the corresponding secondary antibody was incubated for 2 h at room temperature. Finally, the PVDF membrane was washed three times with TBST buffer for 5 min each time, and protein expression was detected by a Chemiluminescence imaging system (Guangzhou BIO-OI Biological Technology Co., Ltd.).

The method of extracting protein from tissue samples is slightly different from the method of extracting protein from cells. First an appropriate amount of tissue was weighed, and then the tissue was placed in a mortar, liquid nitrogen was added, and the tissue was ground gently. In order to prevent protein degradation, liquid nitrogen was constantly added during the entire grinding process until the tissue was ground into a powder without particles. Then 1.0 mL of RIPA lysis buffer containing a cocktail of protease inhibitors and phosphatase inhibitors was added directly into the mortar. After the grinding returned to a normal temperature, the RIPA lysis buffer was collected into a 1.5 mL EP tube, continued to lyse on ice for 30 min, and was gently shaken once every 10 min. The subsequent experiment operation is the same as the method of extracting protein from cells.

Real-Time Quantitative PCR. Total RNA was extracted from the cells or tissue samples using HiScript II Q RT SuperMix for the qPCR mini kit. The cDNA was generated from the total RNAs isolated above according to the manufacturer's instructions. The mRNA expression levels were quantified by RT-qPCR using ChamQ Universal SYBR qPCR Master Mix.

Statistical Analysis. Statistical analysis was performed using an ANOVA test followed by a Bonferroni *posthoc* test (GraphPad Prism) or Student's *t*-test. Data were expressed as mean ± standard error of mean (S.E.M.). Statistical significance was represented by $*P < 0.05$, $**P < 0.01$, and $***P < 0.001$.

ASSOCIATED CONTENT

Supporting Information

The Supporting Information is available free of charge at https://pubs.acs.org/doi/10.1021/acsnano.1c03726.

Supplementary figures include material characterization data, hemocompatibility, cytotoxicity, fluorescence spectroscopic detection, pharmacokinetics, biological distribution, RT-qPCR for CIA and IBD model tissue sample, immunofluorescence, and ELISA; supplementary tables include the sequence of siERN1 and RT-qPCR primer, HSS, and OARSI scores (PDF)

AUTHOR INFORMATION

Corresponding Author

Fengjin Guo − *Department of Cell Biology and Genetics, Core Facility of Development Biology, Chongqing Medical University, Chongqing 400016, China;* orcid.org/0000-0002-7414-6585; Phone: +86 15310288670; Email: guo.fengjin@gmail.com, guo.fengjin@cqmu.edu.cn

Authors

Naibo Feng − *Department of Cell Biology and Genetics, Core Facility of Development Biology, Chongqing Medical University, Chongqing 400016, China*

Li Liang − *Department of Cell Biology and Genetics, Core Facility of Development Biology, Chongqing Medical University, Chongqing 400016, China*

Mengtian Fan − *Department of Cell Biology and Genetics, Core Facility of Development Biology, Chongqing Medical University, Chongqing 400016, China*

Yu Du − *Department of Orthopedics, The 2nd Affiliated Hospital of Chongqing Medical University, Chongqing 400016, China*

Cheng Chen − *Department of Orthopedics, The 1st Affiliated Hospital of Chongqing Medical University, Chongqing 400016, China*

Rong Jiang − *Laboratory of Stem Cells and Tissue Engineering, Chongqing Medical University, Chongqing 400016, China*

Dongsheng Yu − *Department of Cell Biology and Genetics, Core Facility of Development Biology, Chongqing Medical University, Chongqing 400016, China*

Yuyou Yang − *Department of Cell Biology and Genetics, Core Facility of Development Biology, Chongqing Medical University, Chongqing 400016, China*

Mengying Zhang − *Department of Cell Biology and Genetics, Core Facility of Development Biology, Chongqing Medical University, Chongqing 400016, China*

Lin Deng − *Department of Cell Biology and Genetics, Core Facility of Development Biology, Chongqing Medical University, Chongqing 400016, China*

Xingyue Li − *Department of Cell Biology and Genetics, Core Facility of Development Biology, Chongqing Medical University, Chongqing 400016, China*

Nana Geng − *Department of Cell Biology and Genetics, Core Facility of Development Biology, Chongqing Medical University, Chongqing 400016, China*

Menglin Xian − *Department of Cell Biology and Genetics, Core Facility of Development Biology, Chongqing Medical University, Chongqing 400016, China*

Qizhong Qin − *Department of Cell Biology and Genetics, Core Facility of Development Biology, Chongqing Medical University, Chongqing 400016, China*

Xiaoli Li − *Department of Cell Biology and Genetics, Core Facility of Development Biology, Chongqing Medical University, Chongqing 400016, China*

Qiaoyan Tan − *Department of Wound Repair and Rehabilitation Medicine, State Key Laboratory of Trauma, Burns and Combined Injury, Trauma Center, Research Institute of Surgery, Daping Hospital, Army Medical University, Chongqing 400042, China*

Fengtao Luo − *Department of Wound Repair and Rehabilitation Medicine, State Key Laboratory of Trauma, Burns and Combined Injury, Trauma Center, Research Institute of Surgery, Daping Hospital, Army Medical University, Chongqing 400042, China*

Fangzhou Song − *Department of Biochemistry and Molecular Biology, Chongqing Medical University, Chongqing 400016, China*

Huabing Qi − *Department of Wound Repair and Rehabilitation Medicine, State Key Laboratory of Trauma, Burns and Combined Injury, Trauma Center, Research Institute of Surgery, Daping Hospital, Army Medical University, Chongqing 400042, China*

Yangli Xie − *Department of Wound Repair and Rehabilitation Medicine, State Key Laboratory of Trauma, Burns and Combined Injury, Trauma Center, Research Institute of*

https://doi.org/10.1021/acsnano.1c03726
ACS Nano XXXX, XXX, XXX−XXX

Surgery, Daping Hospital, Army Medical University, Chongqing 400042, China

Complete contact information is available at: https://pubs.acs.org/10.1021/acsnano.1c03726

Author Contributions

The manuscript was written through contributions of all authors. All authors have given approval to the final version of the manuscript. F.J.G. and N.B.F. designed experiments; N.B.F., L.L, M.T.F., R.J., Y.Y.Y., M.Y.Z., L.D., X.Y.L., N.N.G., M.L.X., and Q.Z.Q. carried out experiments; N.B.F., D.S.Y., X.L.L., Q.Y.T., F.T.L., F.Z.S., H.B.Q., Y.L.X., and F.J.G. analyzed data; Y.D. and C.C. provided the cartilage tissues of OA and RA patients, and F.Z.S. gave us good advice on the interpretation of data. F.J.G. designed the manuscript and had full access to all of the data in the study and takes responsibility for the integrity of the data and the accuracy of the data analysis. All authors approved the final manuscript prior to submission.

Notes

The authors declare no competing financial interest.

ACKNOWLEDGMENTS

Our experiments were supported by Natural Science Foundation of China (No. 81672209, No. 81871769); Chongqing Science and Technology Bureau (cstc2020jcyj-msxmX0175); and Chongqing Human Resources and Social Security Bureau (2018-389). All experiments were completed on the experimental platform provided by the Core Facility of Development Biology of Basic Medical College (Chongqing Medical University). We are especially grateful to Nanjing Nanoeast Biotech Co., Ltd. for its guidance and assistance in the synthesis of materials for this study.

REFERENCES

(1) Wang, L.; Wang, F. S.; Gershwin, M. E. Human Autoimmune Diseases: A Comprehensive Update. *J. Intern. Med.* **2015**, *278* (4), 369−395.

(2) Goldblatt, F.; O'Neill, S. G. Clinical Aspects of Autoimmune Rheumatic Diseases. *Lancet* **2013**, *382* (9894), 797−808.

(3) Zhernakova, A.; Withoff, S.; Wijmenga, C. Clinical Implications of Shared Genetics and Pathogenesis in Autoimmune Diseases. *Nat. Rev. Endocrinol.* **2013**, *9* (11), 646−659.

(4) Cho, J. H.; Feldman, M. Heterogeneity of Autoimmune Diseases: Pathophysiologic Insights from Genetics and Implications for New Therapies. *Nat. Med.* **2015**, *21* (7), 730−738.

(5) Smolen, J. S.; Landewé, R. B. M.; Bijlsma, J. W. J.; Burmester, G. R.; Dougados, M.; Kerschbaumer, A.; McInnes, I. B.; Sepriano, A.; van Vollenhoven, R. F.; de Wit, M.; Aletaha, D.; Aringer, M.; Askling, J.; Balsa, A.; Boers, M.; den Broeder, A. A.; Buch, M. H.; Buttgereit, F.; Caporali, R.; Cardiel, M. H.; et al. Eular Recommendations for the Management of Rheumatoid Arthritis with Synthetic and Biological Disease-Modifying Antirheumatic Drugs: 2019 Update. *Ann. Rheum. Dis.* **2020**, *79* (6), 685−699.

(6) Onuora, S. Eular Updates Its RA Management Recommendations. *Nat. Rev. Rheumatol.* **2020**, *16* (3), 128.

(7) Scott, D. L. Interstitial Lung Disease and Disease Modifying Anti-Rheumatic Drugs. *Lancet* **2004**, *363* (9416), 1239−1240.

(8) Richards, J. S.; Dowell, S. M.; Quinones, M. E.; Kerr, G. S. How to Use Biologic Agents in Patients with Rheumatoid Arthritis Who Have Comorbid Disease. *Bmj* **2015**, *351*, No. h3658.

(9) Ravindran, V.; Scott, D. L.; Choy, E. H. A Systematic Review and Meta-Analysis of Efficacy and Toxicity of Disease Modifying Anti-Rheumatic Drugs and Biological Agents for Psoriatic Arthritis. *Ann. Rheum. Dis.* **2008**, *67* (6), 855−859.

(10) Hetz, C.; Chevet, E.; Harding, H. P. Targeting the Unfolded Protein Response in Disease. *Nat. Rev. Drug Discovery* **2013**, *12* (9), 703−719.

(11) Grootjans, J.; Kaser, A.; Kaufman, R. J.; Blumberg, R. S. The Unfolded Protein Response in Immunity and Inflammation. *Nat. Rev. Immunol.* **2016**, *16* (8), 469−484.

(12) Hetz, C.; Zhang, K.; Kaufman, R. J. Mechanisms, Regulation and Functions of the Unfolded Protein Response. *Nat. Rev. Mol. Cell Biol.* **2020**, *21* (8), 421−438.

(13) Keestra-Gounder, A. M.; Byndloss, M. X.; Seyffert, N.; Young, B. M.; Chávez-Arroyo, A.; Tsai, A. Y.; Cevallos, S. A.; Winter, M. G.; Pham, O. H.; Tiffany, C. R.; de Jong, M. F.; Kerrinnes, T.; Ravindran, R.; Luciw, P. A.; McSorley, S. J.; Bäumler, A. J.; Tsolis, R. M. NOD1 and NOD2 Signalling Links ER Stress with Inflammation. *Nature* **2016**, *532* (7599), 394−397.

(14) Wheeler, M. A.; Jaronen, M.; Covacu, R.; Zandee, S. E. J.; Scalisi, G.; Rothhammer, V.; Tjon, E. C.; Chao, C. C.; Kenison, J. E.; Blain, M.; Rao, V. T. S.; Hewson, P.; Barroso, A.; Gutiérrez-Vázquez, C.; Prat, A.; Antel, J. P.; Hauser, R.; Quintana, F. J. Environmental Control of Astrocyte Pathogenic Activities in CNS Inflammation. *Cell* **2019**, *176* (3), 581−596.

(15) Qiu, Q.; Zheng, Z.; Chang, L.; Zhao, Y. S.; Tan, C.; Dandekar, A.; Zhang, Z.; Lin, Z.; Gui, M.; Li, X.; Zhang, T.; Kong, Q.; Li, H.; Chen, S.; Chen, A.; Kaufman, R. J.; Yang, W. L.; Lin, H. K.; Zhang, D.; Perlman, H.; et al. Toll-Like Receptor-Mediated IRE1α Activation as a Therapeutic Target for Inflammatory Arthritis. *EMBO J.* **2013**, *32* (18), 2477−2490.

(16) Yin, Q.; Shen, J.; Chen, L.; Zhang, Z.; Gu, W.; Li, Y. Overcoming Multidrug Resistance by Co-Delivery of MDR-1 and Survivin-Targeting RNA with Reduction-Responsible Cationic Poly(B-Amino Esters). *Biomaterials* **2012**, *33* (27), 6495−6506.

(17) Tzeng, S. Y.; Hung, B. P.; Grayson, W. L.; Green, J. J. Cystamine-Terminated Poly(Beta-Amino Ester)S for siRNA Delivery to Human Mesenchymal Stem Cells and Enhancement of Osteogenic Differentiation. *Biomaterials* **2012**, *33* (32), 8142−8151.

(18) Han, L.; Zhao, J.; Zhang, X.; Cao, W.; Hu, X.; Zou, G.; Duan, X.; Liang, X. J. Enhanced siRNA Delivery and Silencing Gold-Chitosan Nanosystem with Surface Charge-Reversal Polymer Assembly and Good Biocompatibility. *ACS Nano* **2012**, *6* (8), 7340−7351.

(19) Ping, Y.; Liu, C.; Zhang, Z.; Liu, K. L.; Chen, J.; Li, J. Chitosan-Graft-(Pei-B-Cyclodextrin) Copolymers and Their Supramolecular Pegylation for DNA and siRNA Delivery. *Biomaterials* **2011**, *32* (32), 8328−8341.

(20) Murray, P. J. Macrophage Polarization. *Annu. Rev. Physiol.* **2017**, *79*, 541−566.

(21) Sica, A.; Mantovani, A. Macrophage Plasticity and Polarization: *In Vivo* Veritas. *J. Clin. Invest.* **2012**, *122* (3), 787−795.

(22) Locati, M.; Curtale, G.; Mantovani, A. Diversity, Mechanisms, and Significance of Macrophage Plasticity. *Annu. Rev. Pathol.: Mech. Dis.* **2020**, *15*, 123−147.

(23) Meli, V. S.; Veerasubramanian, P. K.; Atcha, H.; Reitz, Z.; Downing, T. L.; Liu, W. F. Biophysical Regulation of Macrophages in Health and Disease. *J. Leukocyte Biol.* **2019**, *106* (2), 283−299.

(24) Biswas, S. K.; Chittezhath, M.; Shalova, I. N.; Lim, J. Y. Macrophage Polarization and Plasticity in Health and Disease. *Immunol. Res.* **2012**, *53* (1−3), 11−24.

(25) Sun, S.; Shi, G.; Sha, H.; Ji, Y.; Han, X.; Shu, X.; Ma, H.; Inoue, T.; Gao, B.; Kim, H.; Bu, P.; Guber, R. D.; Shen, X.; Lee, A. H.; Iwawaki, T.; Paton, A. W.; Paton, J. C.; Fang, D.; Tsai, B.; Yates, J. R., 3rd; et al. IRE1α Is an Endogenous Substrate of Endoplasmic-Reticulum-Associated Degradation. *Nat. Cell Biol.* **2015**, *17* (12), 1546−1555.

(26) Shan, B.; Wang, X.; Wu, Y.; Xu, C.; Xia, Z.; Dai, J.; Shao, M.; Zhao, F.; He, S.; Yang, L.; Zhang, M.; Nan, F.; Li, J.; Liu, J.; Liu, J.; Jia, W.; Qiu, Y.; Song, B.; Han, J. J.; Rui, L.; et al. The Metabolic ER Stress Sensor IRE1α Suppresses Alternative Activation of Macrophages and Impairs Energy Expenditure in Obesity. *Nat. Immunol.* **2017**, *18* (5), 519−529.

(27) Oubaha, M.; Miloudi, K.; Dejda, A.; Guber, V.; Mawambo, G.; Germain, M. A.; Bourdel, G.; Popovic, N.; Rezende, F. A.; Kaufman, R.

J.; Mallette, F. A.; Sapieha, P. Senescence-Associated Secretory Phenotype Contributes to Pathological Angiogenesis in Retinopathy. *Sci. Transl. Med.* **2016**, *8* (362), 362ra144.
(28) Bernkop-Schnürch, A. Strategies to Overcome the Polycation Dilemma in Drug Delivery. *Adv. Drug Delivery Rev.* **2018**, *136*−*137*, 62−72.
(29) Fearon, U.; Canavan, M.; Biniecka, M.; Veale, D. J. Hypoxia, Mitochondrial Dysfunction and Synovial Invasiveness in Rheumatoid Arthritis. *Nat. Rev. Rheumatol.* **2016**, *12* (7), 385−397.
(30) Udalova, I. A.; Mantovani, A.; Feldmann, M. Macrophage Heterogeneity in the Context of Rheumatoid Arthritis. *Nat. Rev. Rheumatol.* **2016**, *12* (8), 472−485.
(31) Chandrupatla, D.; Molthoff, C. F. M.; Lammertsma, A. A.; van der Laken, C. J.; Jansen, G. The Folate Receptor B as a Macrophage-Mediated Imaging and Therapeutic Target in Rheumatoid Arthritis. *Drug Delivery Transl. Res.* **2019**, *9* (1), 366−378.
(32) Friedman, B.; Cronstein, B. Methotrexate Mechanism in Treatment of Rheumatoid Arthritis. *Jt., Bone, Spine* **2019**, *86* (3), 301−307.
(33) Yang, Y.; Guo, L.; Wang, Z.; Liu, P.; Liu, X.; Ding, J.; Zhou, W. Targeted Silver Nanoparticles for Rheumatoid Arthritis Therapy *via* Macrophage Apoptosis and Re-Polarization. *Biomaterials* **2021**, *264*, 120390.
(34) Laidlaw, B. J.; Craft, J. E.; Kaech, S. M. The Multifaceted Role of CD4(+) T Cells in CD8(+) T Cell Memory. *Nat. Rev. Immunol.* **2016**, *16* (2), 102−111.
(35) Huang, B.; Wang, Q. T.; Song, S. S.; Wu, Y. J.; Ma, Y. K.; Zhang, L. L.; Chen, J. Y.; Wu, H. X.; Jiang, L.; Wei, W. Combined Use of Etanercept and MTX Restores $CD4^+/CD8^+$ Ratio and Tregs in Spleen and Thymus in Collagen-Induced Arthritis. *Inflammation Res.* **2012**, *61* (11), 1229−1239.
(36) Liebold, I.; Grützkau, A.; Göckeritz, A.; Gerl, V.; Lindquist, R.; Feist, E.; Zänker, M.; Häupl, T.; Poddubnyy, D.; Zernicke, J.; Smiljanovic, B.; Alexander, T.; Burmester, G. R.; Gay, S.; Stuhlmüller, B. Peripheral Blood Mononuclear Cells Are Hypomethylated in Active Rheumatoid Arthritis and Methylation Correlates with Disease Activity. *Rheumatology (Oxford, U. K.)* **2021**, *60* (4), 1984−1995.
(37) Komatsu, N.; Okamoto, K.; Sawa, S.; Nakashima, T.; Oh-Hora, M.; Kodama, T.; Tanaka, S.; Bluestone, J. A.; Takayanagi, H. Pathogenic Conversion of Foxp3+ T Cells into Th17 Cells in Autoimmune Arthritis. *Nat. Med.* **2014**, *20* (1), 62−68.
(38) Jin, S.; Chen, H.; Li, Y.; Zhong, H.; Sun, W.; Wang, J.; Zhang, T.; Ma, J.; Yan, S.; Zhang, J.; Tian, Q.; Yang, X.; Wang, J. Maresin 1 Improves the Treg/Th17 Imbalance in Rheumatoid Arthritis through MiR-21. *Ann. Rheum. Dis.* **2018**, *77* (11), 1644−1652.
(39) Ohkura, N.; Sakaguchi, S. Transcriptional and Epigenetic Basis of Treg Cell Development and Function: Its Genetic Anomalies or Variations in Autoimmune Diseases. *Cell Res.* **2020**, *30* (6), 465−474.
(40) Paradowska-Gorycka, A.; Wajda, A.; Romanowska-Próchnicka, K.; Walczuk, E.; Kuca-Warnawin, E.; Kmiolek, T.; Stypinska, B.; Rzeszotarska, E.; Majewski, D.; Jagodzinski, P. P.; Pawlik, A. Th17/Treg-Related Transcriptional Factor Expression and Cytokine Profile in Patients with Rheumatoid Arthritis. *Front. Immunol.* **2020**, *11*, 572858.
(41) Carreras-Sureda, A.; Jaña, F.; Urra, H.; Durand, S.; Mortenson, D. E.; Sagredo, A.; Bustos, G.; Hazari, Y.; Ramos-Fernández, E.; Sassano, M. L.; Pihán, P.; van Vliet, A. R.; González-Quiroz, M.; Torres, A. K.; Tapia-Rojas, C.; Kerkhofs, M.; Vicente, R.; Kaufman, R. J.; Inestrosa, N. C.; Gonzalez-Billault, C.; et al. Non-Canonical Function of IRE1α Determines Mitochondria-Associated Endoplasmic Reticulum Composition to Control Calcium Transfer and Bioenergetics. *Nat. Cell Biol.* **2019**, *21* (6), 755−767.
(42) Malli, R.; Graier, W. F. IRE1α Modulates ER and Mitochondria Crosstalk. *Nat. Cell Biol.* **2019**, *21* (6), 667−668.
(43) Son, S. M.; Byun, J.; Roh, S. E.; Kim, S. J.; Mook-Jung, I. Reduced Ire1α Mediates Apoptotic Cell Death by Disrupting Calcium Homeostasis *via* the InsP3 Receptor. *Cell Death Dis.* **2014**, *5* (4), No. e1188.
(44) Schappe, M. S.; Szteyn, K.; Stremska, M. E.; Mendu, S. K.; Downs, T. K.; Seegren, P. V.; Mahoney, M. A.; Dixit, S.; Krupa, J. K.; Stipes, E. J.; Rogers, J. S.; Adamson, S. E.; Leitinger, N.; Desai, B. N. Chanzyme Trpm7Mediates the Ca(2+) Influx Essential for Lipopolysaccharide-Induced Toll-Like Receptor 4 Endocytosis and Macrophage Activation. *Immunity* **2018**, *48* (1), 59−74.
(45) Tedesco, S.; Scattolini, V.; Albiero, M.; Bortolozzi, M.; Avogaro, A.; Cignarella, A.; Fadini, G. P. Mitochondrial Calcium Uptake Is Instrumental to Alternative Macrophage Polarization and Phagocytic Activity. *Int. J. Mol. Sci.* **2019**, *20* (19), 4966.
(46) Nie, H.; Zheng, Y.; Li, R.; Guo, T. B.; He, D.; Fang, L.; Liu, X.; Xiao, L.; Chen, X.; Wan, B.; Chin, Y. E.; Zhang, J. Z. Phosphorylation of Foxp3 Controls Regulatory T Cell Function and Is Inhibited by TNF-α in Rheumatoid Arthritis. *Nat. Med.* **2013**, *19* (3), 322−328.
(47) Roberts, C. A.; Dickinson, A. K.; Taams, L. S. The Interplay between Monocytes/Macrophages and CD4(+) T Cell Subsets in Rheumatoid Arthritis. *Front. Immunol.* **2015**, *6*, 571.
(48) Li, Z.; Li, D.; Tsun, A.; Li, B. Foxp3+ Regulatory T Cells and Their Functional Regulation. *Cell. Mol. Immunol.* **2015**, *12* (5), 558−565.
(49) Takeuchi, O.; Hoshino, K.; Akira, S. Cutting Edge: TLR2-Deficient and Myd88-Deficient Mice Are Highly Susceptible to *Staphylococcus aureus* Infection. *J. Immunol.* **2000**, *165* (10), 5392−5396.
(50) Feng, N.; Yang, M.; Feng, X.; Wang, Y.; Chang, F.; Ding, J. Reduction-Responsive Polypeptide Nanogel for Intracellular Drug Delivery in Relieving Collagen-Induced Arthritis. *ACS Biomater. Sci. Eng.* **2018**, *4* (12), 4154−4162.

https://doi.org/10.1021/acsnano.1c03726
ACS Nano XXXX, XXX, XXX−XXX